Design of a Benchtop Facility for Parametric Evaluation of Engine Oil Quality

By
Adam David Smith

Thesis
Submitted to the Faculty of the
Graduate School of Vanderbilt University
in partial fulfillment of the requirements
for the degree of

MASTER OF SCIENCE
in
MECHANICAL ENGINEERING

MAY 31, 2021
Nashville, Tennessee

Approved:
Amrutur V. Anilkumar, Ph.D.
Gautam Biswas, Ph.D.
Haoxiang Luo, Ph.D.

ACKNOWLEDGMENTS

I would like to offer my special gratitude to my advisor Dr. Amrutur Anilkumar for his steadfast support, patience, and mentorship over the past few years. Your insight and feedback have been instrumental in sharpening my thinking and expanding my abilities as an engineer and researcher. Additionally, I would like to thank Dr. Gautam Biswas for his perspective and support that made this work possible and Dr. Haoxiang Luo for his advice and knowledge as a teacher and member of my committee.

I would also like to thank Robin Midgett for always willing to lend a helping hand, Phil Davis for always taking the time to provide practical guidance, and Tim Darrah, Yubo Du, and Nisala Kalupahana for their software assistance.

I offer my sincere appreciation to my friends for their continuous encouragement and belief in me. Finally, for their unwavering support of my educational and personal goals, I would especially like to thank my family.

TABLE OF CONTENTS

LIST OF FIGURES

LIST OF TABLES

LIST OF ABBREVIATIONS

ASTM American Society of Testing and Materials. 6

BSPP British Standard Parallel Pipe. 4

EMI Electromagnetic Interference. 23

ESR equivalent series resistor. 9

HMS Health Monitoring System. 1

IEC International Electrotechnical Commission. 23

NIST National Institute of Standards and Technology. 23

NPT National Pipe Thread. 23

OQS Oil Quality Sensor. 4

P&ID piping and instrumentation diagram. 14

PID proportional-integral-derivative. 12

PTFE polytetrafluoroethylene. 21

RTD Resistance Temperature Detector. 11

SAE Society of Automotive Engineers. 5

SVR Support Vector Regression. 55

VI viscosity index. 5

CHAPTER ONE

INTRODUCTION

1.1 Motivation

The focus of this study is real time *in situ* monitoring of engine oil quality through the parametric evaluation of instrumentation performance, and examination of the quality and reliability of measurements, through the development of a benchtop engine oil test facility.

Overall automotive engine performance is strongly dependent on the working quality of the oil that degrades with use due to the high-friction, high-temperature lubricating environment. Oil degradation leads to chemical and physical property changes that in turn cause more stressful engine operation. For land-based vehicles, statistically-determined mileages are used to recommend oil changes, though real-time monitoring of oil quality would be the preferred option [1].

Traditionally, oil quality has been analyzed through laboratory tests such as ferrography, mass spectroscopy, chemical tests, and viscosity measurements that usually require a sample of oil to be analyzed offline [2]. These tests are relatively widespread and used in commercial applications. The problem of real time engine oil quality monitoring, where a user can get continuous feedback, has been the focus of extensive research in recent years [1, 2, 3, 4, 5, 6, 7, 8] for its potential economic and environmental implications. This has led to the development of various technologies [2, 4], automated approaches [9], and machine learning models [10]. These technologies can only be deemed suitable for the end use application after being systematically studied over the entire range of engine operating conditions.

The requirement of *in situ* oil quality sensing becomes all the more important for marine vehicles, as unlike land-based vehicles there is not a simple distance or time standard that can accurately cover oil change protocols.

This work is motivated by the desire of the U.S. Navy to develop an engine health monitoring system (HMS) for a fleet of manned and unmanned combatant craft. The HMS proposes to use a data-driven approach to both diagnose and predict abnormalities in the

operation of the craft using a combination of hardware and software tools. This approach intends to reduce operational cost, reduce maintenance intervals, and provide a platform for future failure mode mitigation and overall system performance studies and ensure the well-being of the craft and personnel in critical environments. The initial stages of this project focus on a potential HMS for Cummins diesel engine-powered speed boats. These boats undergo short missions, but the engines may experience a wide range of operating conditions, from smooth, continuous operation to high-acceleration, high-speed, or high-torque maneuvers, exacerbated by the random, dynamic loading on the craft due to wave impacts. The engine oil degradation is heavily dependent on the particular operation of the boat. Through real-time or pseudo-real time monitoring, the Navy intends to implement a more customized oil changeout approach.

1.2 Background

Lubricating oil follows a complex path through the engine, beginning in the sump, a low point where the oil collects when the engine is not operating. During operation, a gear pump, mechanically driven by the engine's gear train, moves the oil toward the filter, with the flow rate proportional to the rotation of the engine. After moving through the filter, oil enters galleries within the engine, where it is pushed up into the cylinder head to lubricate the camshaft, camshaft bearings, push rods, and rocker arms. It is also pushed down to the spinning crankshaft, lubricating its bearings. Most importantly, the cylinder wall-piston interface is lubricated by upward splashing of the crankcase oil, and this is harshest environment encountered by the oil. In some engines, the connecting rod has holes for jet lubrication of the cylinder wall. To complete the cycle, oil falls back into the sump due to gravity.

The piston-cylinder interface exposes the oil to high temperatures and high pressures, locally, that accelerate oxidation. Here, the oil is also exposed to wear debris from the metal-to-metal contacts, and moisture and combustion products through imperfect piston ring seals [12, 13].

A testbed engine in the Energetics Laboratory at Vanderbilt University was modified for comparative engine health monitoring studies with the Navy speedboat Cummins diesel engines (Figure 1.2). The testbed engine is a Volkswagen 4-cylinder, 1.9L TDI diesel engine equipped with common vehicle instrumentation and an OBD port and a controllable KLAM K40 eddy-current dynamometer to provide a resistive load capable of producing a nominal 44 kW at 3600 rpm and a nominal torque of 130 Nm at 2200 rpm.

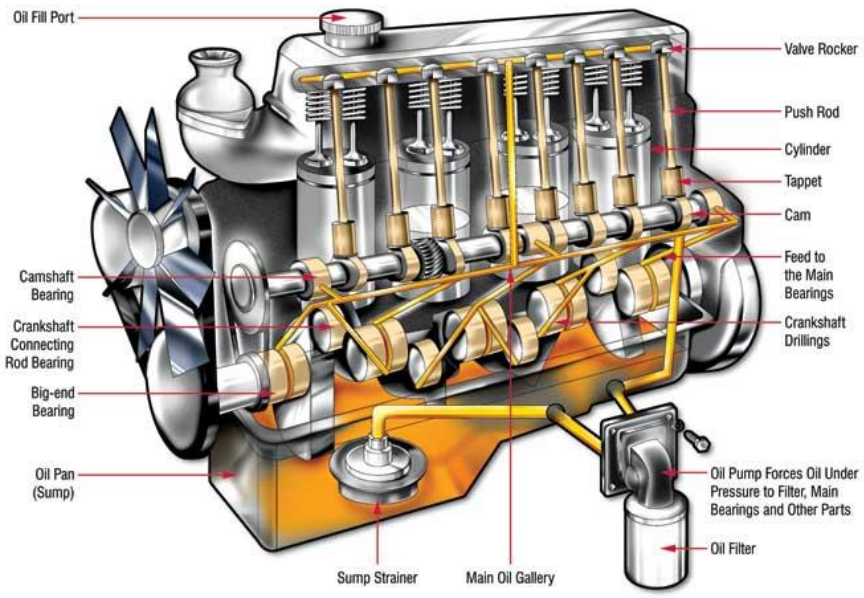

Figure 1.1 General schematic of engine lubrication system [11]

.

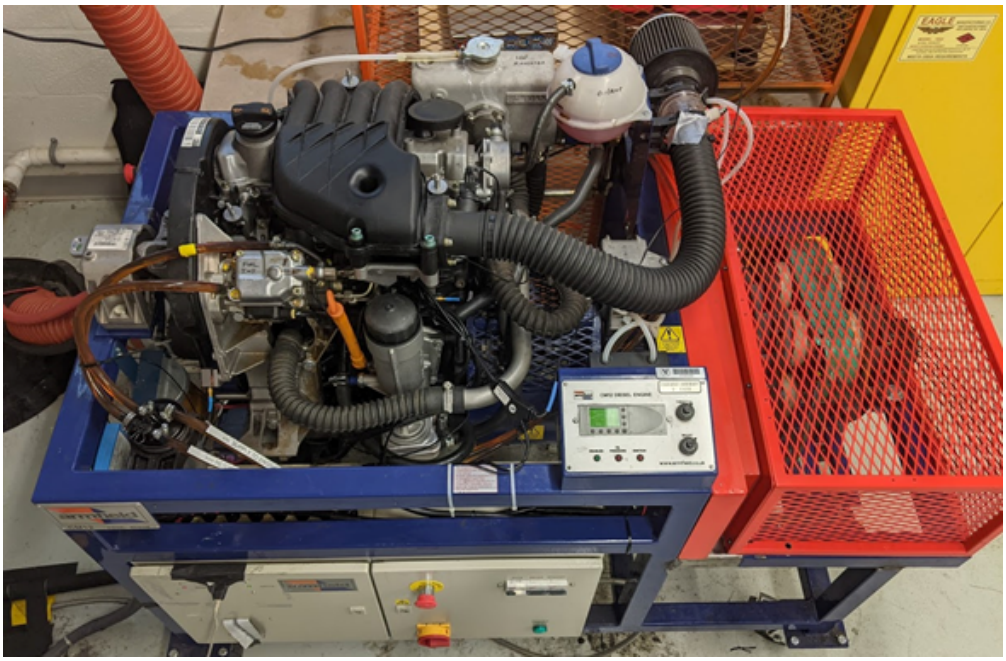

Figure 1.2 Testbed Volkswagen 4-cylinder, 1.9L TDI diesel engine with dynamometer.

For this project, the testbed engine was modified to accommodate two Dytran

5384 accelerometers and a Tan Delta GenII Oil Quality Sensor (OQS) (Section 1.7). The accelerometers were installed on opposite sides of the engine to be used for planned studies correlating oil quality with engine vibration.

The OQS was installed on the oil filter housing immediately downstream of the filter, as this was the only location possible to intercept the oil path without making drastic modifications to the engine block itself (Figure 1.3). A custom $1/2''$ (BSPP) threaded section aluminum tube was concentrically welded around a hole drilled into the top plane of the part. In this configuration, the OQS is angled 15° from vertical and the probe tip intercepts the oil flow leaving the filter and filter bypass without obstructing the flow.

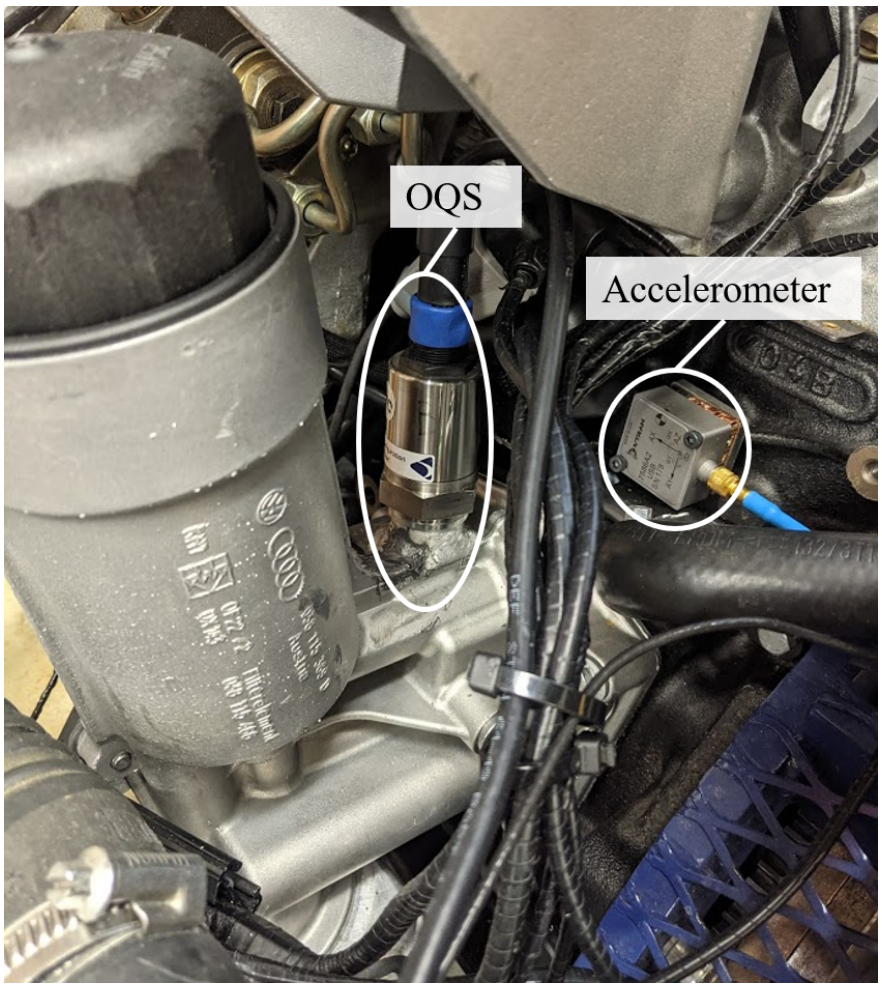

Figure 1.3 Location of the OQS on the modified oil filter housing.

A parametric evaluation of the OQS with respect to engine operating conditions of oil temperature, pressure, flow rate, and sensor spatial orientation cannot be conducted using the engine. The engine oil parameters cannot be independently controlled, as they are tied to the engine speed and load, making it difficult to run controlled experiments. Further, monitoring oil quality degradation through continuous testbed engine use is an extensive process, requiring hundreds of hours of operation to degrade the oil, incurring high fuel costs, downtime due to maintenance, and excessive man-hours of operation.

A benchtop test facility has been designed to conduct parametric evaluation of the OQS under controlled conditions. Such a facility must be capable of replicating the oil conditions found in the engine and also have the ability to independently control the parameters required for scientific analysis. It also must ensure measurement accuracy and repeatability, not contribute to further oil degradation during the course of a study, and guarantee safe operation.

1.3 Engine Oil Properties

Engine oil differs from other types of industrial lubricants in that it is designed to be exposed to the high working temperatures and pressures of an engine. Additives such as antioxidants, dispersants, detergents, anti-wear agents, foam inhibitors, friction modifiers, pour-point depressants, and viscosity index (VI) improvers are added to extend the operational range and life of the oil [14].Contemporary base oils are synthetic. Synthetic oils are most commonly composed of a uniform hydrocarbon structure of chemically modified products from distilled petroleum. Synthetic oils have become the norm in engines for durability and extended resistance to oxidative degradation [15].

Despite all of these modifications, engine oil can still be characterized in the physical space through the physical properties of viscosity and density. Engine oils are multigrade and are assigned an Society of Automotive Engineers (SAE) viscosity grade at cold temperatures, typically 0 °C, and operating temperatures, typically 100 °C. Multigrade oils are assigned a label of XW-Y, where X represents the viscosity at cold temperatures and Y represents the viscosity at operating temperatures. The two values refer to the "weight" of the oil, a commonplace number that represents a given range of viscosity values. For example, a 5W-30 oil will be less viscous than a 10W-30 oil at cold temperatures, and a 5W-40 oil will be more viscous than a 5W-30 oil at operating temperatures. Diesel engine oils are typically more viscous than spark ignition oils due to the more extreme conditions that they

are exposed to.

Manufacturers provide datasheets that include the measured kinematic viscosity at two standard temperatures, 40 °C and 100 °C, and the measured density at 15 °C and ambient pressure. As set forth by the American Society of Testing and Materials (ASTM), these values can be used as reference points in calculating the viscosity and density of the oil at other temperatures. Generally, since these oils are incompressible, pressure does not influence either viscosity or density. Also provided is the oil's flash point, which is helpful in designing a safe system. With an effective engine cooling system, the maximum operating temperature for a diesel engine oil is about 115 °C (240 °F).

Walther's equation is a widely accepted engine oil viscosity model and is presented in the form shown in Equation 1.1, where ν is the kinematic viscosity and T is the temperature in units of °C. This equation forms the basis for the ASTM D341 standard [16].

$$log_{10}(log_{10}(\nu - \lambda)) = A - Blog_{10}(T), \tag{1.1}$$

where A and B are oil-specific constants and λ is a universal shift constant (approximately 0.7 for engine oils [17]).

Engine oil density is primarily dependent on temperature, as excessive pressures are only locally encountered at lubricating surfaces [18]. Density linearly decreases over the engine operating temperature regime. Using the manufacturer-provided density value ρ_0 at the reference temperature T_0 (15 °C) the density was calculated using Equation 1.2, with T in units of °C.

$$\rho = \rho_0 + (T_0 - T)(0.73\frac{\frac{kg}{m^3}}{^\circ C}) \tag{1.2}$$

1.4 Oil Quality Measurement

While the physical properties of viscosity and density are necessary to characterize an engine oil, they are not sufficient to determine its quality, as in its state of degradation or deterioration following use in the harsh engine environment.

The primary cause for engine oil degradation is the oxidation of the constituent hydrocarbons, a process accelerated by the high temperature and high pressure stresses within the engine, especially at the cylinder-piston interface [19].

The oxidative breakdown of the base oil molecules generates polar molecules, along with insoluble products such as hydroperoxides, alkyl peroxides, alcohols, carboxylic acids,

peroxy acids, esters, ketones, aldehydes and lactones that inhibit the oil's performance. The change in concentration of polar molecules, with engine use, presents a mechanism for *in situ* monitoring of oil quality through electrical permittivity measurements.

1.5 Permittivity Measurement of Oil

The state-of-the-art oil quality sensors directly measure the complex permittivity of the oil. The complex permittivity ε^* consists of a real part ε' and an imaginary part ε''.

$$\varepsilon^* = \varepsilon' - j\varepsilon'' \tag{1.3}$$

The real part of permittivity is a measure of how much energy is stored by a dielectric material in an electric field [20]. The imaginary part of permittivity, or loss factor, is a measure of the energy loss due to the changing polarization of a dielectric in the presence of an applied alternating electric field [20]. For an engine oil that starts clean and is an insulator, the presence of polar molecules due to degradation contributes to the change in the imaginary part of permittivity. This change becomes significant and lays the framework for sensing oil quality through an *in situ* sensor.

1.6 $tan(\delta)$ Sensing

The accepted metric for oil quality studies is the loss tangent, or $tan(\delta)$ value, a ratio of the imaginary part over the real part of permittivity. The real part of permittivity changes very slowly compared to the imaginary part as an oil degrades, leading to an increase in the $tan(\delta)$ value [20].

$$tan(\delta) = \frac{\varepsilon''}{\varepsilon'} \tag{1.4}$$

The $tan(\delta)$ measurements vary with the frequency of the applied electric field of a given sensor. Depending on the sensed media and the sensor design, this sensing frequency occurs from the kHz range to the low MHz range. Figure 1.4 shows the variation of the real part of permittivity as a function of sensing frequency and temperature for transformer oil, showing that the real part of permittivity does not change much with temperature or sensing frequency [20].

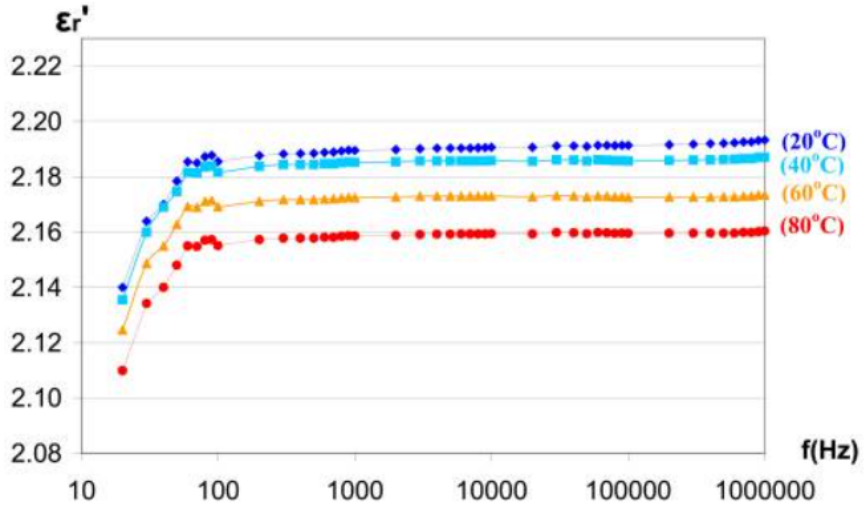

Figure 1.4 Temperature and frequency dependence of the real part of permittivity for transformer oils in a state requiring reconditioning [20]

.

Figure 1.5b shows the variation of the imaginary part of permittivity as a function of sensing frequency and temperature for palm oil [21]. Clearly, there is an optimal frequency window for measurement sensitivity. Figure 1.5a shows the corresponding $tan(\delta)$ value for the oil and demonstrates the capability of the oil quality sensor.

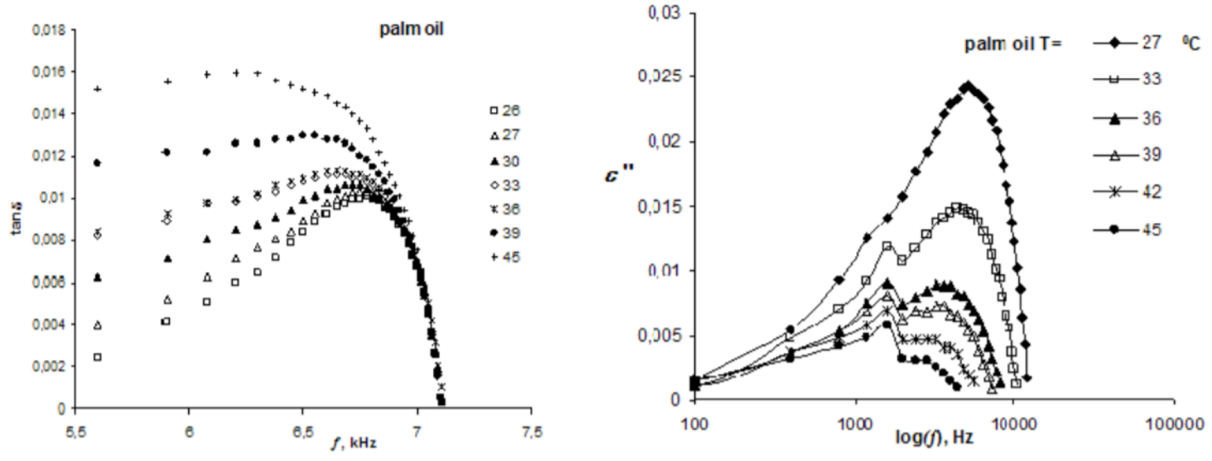

Figure 1.5 Frequency dependence of **(a)** $tan(\delta)$ and **(b)** ε'' at six different temperatures for palm oil [21]

The sensing frequency and the $tan(\delta)$ response associated with the oil quality sensor deployed in the current studies is in the MHz frequency range and is proprietorial information, however, the response will be along the lines shown in Figure 1.4 and Figure 1.5.

1.7 Oil Quality Sensor Design

For simple sensor geometries, expressions can be developed to relate the complex permittivity of the oil to capacitance and impedance measurements [22, 21, 23]. For a cylindrical electrode geometry, a simple circuit of a capacitor and equivalent series resistor (ESR) is used to determine the complex impedance [22]. The image and schematic of the sensing electrodes for the Tan Delta OQSx-GenII sensor used in the current studies are shown in Figure 1.6.

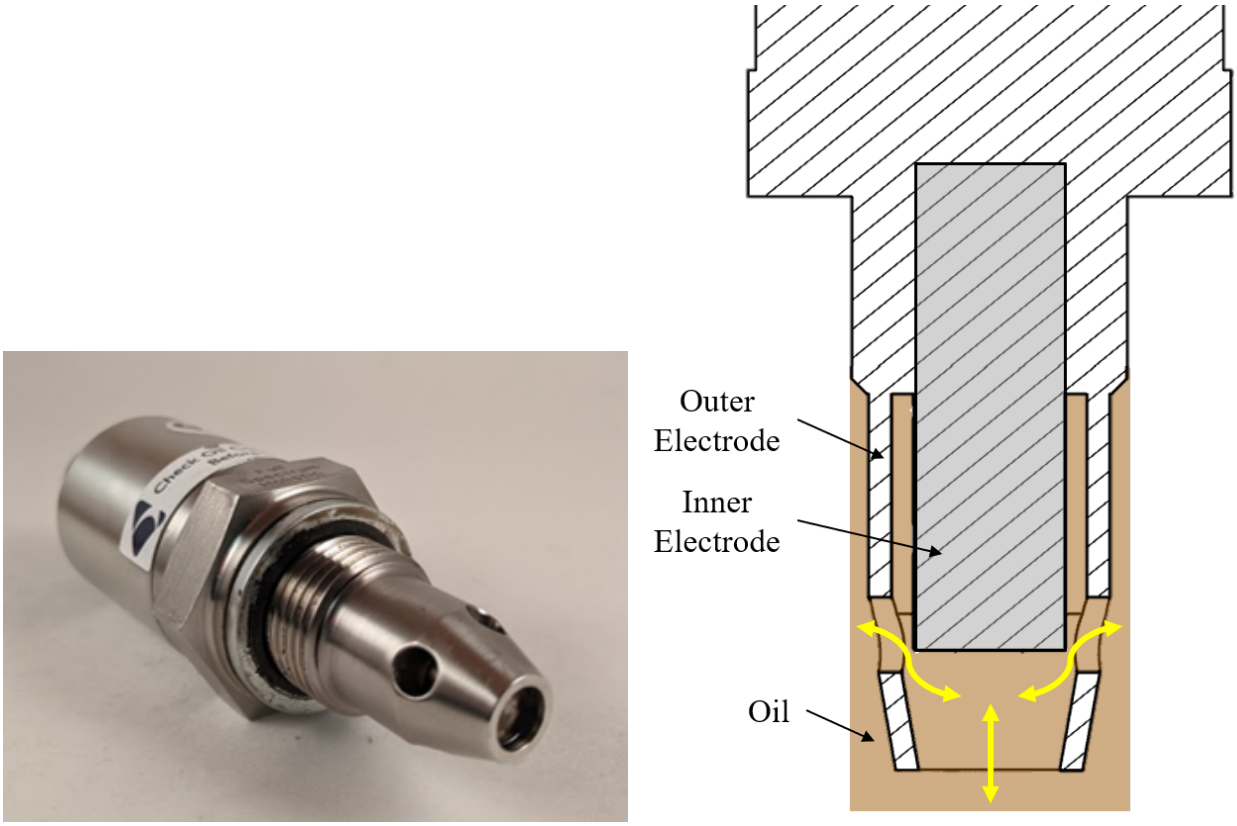

(a) Sensor tip. **(b)** Sensing electrode schematic.

Figure 1.6 Tan Delta OQSx-GenII.

Figure 1.7a captures the *in situ* performance of the select Tan Delta OQSx-GenII sensor in our test facility using a degraded oil. At a constant temperature of 220 °F, typical of engine operation, the sensor shows a steady loss factor value of 6%, whereas a clean oil

would hover around a 0% loss factor. The measured loss factor value is independent of flowrate and has some sensitivity to temperature changes. In an engine environment, with continuous use, the oil will degrade even further and a loss factor of 30% is considered end-of-life. Figure 1.7b shows that the transition from a 6% degraded oil to a 30% degraded oil occurs more rapidly than initial stages of degradation starting from a clean oil [24].

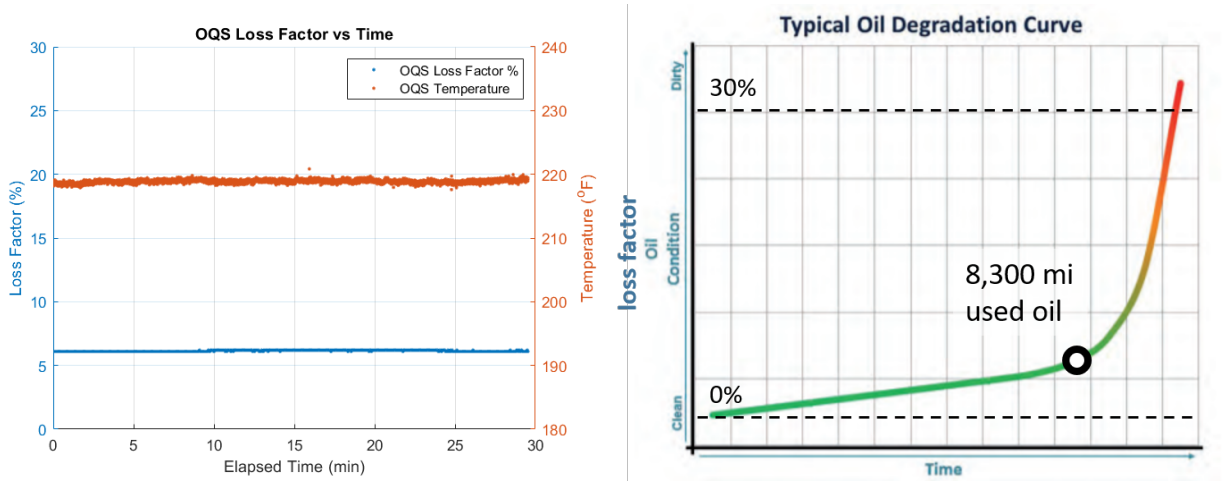

(a) OQS loss factor measurements for a degraded oil.

(b) Typical engine oil degradation curve with the tested degraded oil [24]

Figure 1.7 *In situ* performance of the OQSx-GenII for a degraded oil.

The focus of this study is to validate the performance of an oil quality sensor under conditions of temperature, orientation, flow rate, with oils of different levels of degradation. The emphasis of this study is on measurement consistency, accuracy, and the ability to project results to engine operating conditions.

CHAPTER TWO

FACILITY DESIGN AND CHARACTERIZATION

2.1 Existing Benchtop Facilities

Some preliminary oil quality studies have been conducted using pump-driven loops to examine the response of a novel oil quality sensor design [4]. The facility design featured PVC tubes, a gear pump, and sensors to monitor the temperature, pressure, and flow rate of the oil. However, this facility was limited in scope because it could not duplicate engine operating temperatures.

A higher temperature circulating loop was developed by [25] to test the heat transfer capabilities of base oil nanofluids with potential lubricative benefits as an oil additive. This test setup featured both a 1500 W preheater and a heat exchanger that could regulate temperatures up to 100 °C.

A more robust study was conducted to measure the pressure drop across orifices for high viscosity fluids that featured a well-instrumented loop [26]. Through the use of a plunger pump and bypass valves, the flow rate and pressure of the working fluid could be controlled. Temperature control was achieved through the use of shell-and-tube and tube-in-tube heat exchangers for temperatures between -25 °C and 50 °C with a chiller providing the heat exchange fluid, and a plate heat exchanger connected to running water for heat rejection. Positive displacement flow meters were used to measure the flow rates. Temperature was measured using three-wire RTD sensors with an accuracy of ±0.6 °C, and high-accuracy (±0.075% of the span in the 0-68,948 kPa range) absolute pressure transducers were used across the orifice.

A circulating loop for engine oil was developed by [27] with a focus on evaluating automobile engine oil filter performance. This facility utilized a gear pump and heater to control two independent loops for different oil types. Each independent loop featured pressure, temperature, and flow rate sensors to monitor the flow characteristics of the oil and filter performance. However, the operating temperature of the system does not appear to be

able to fully replicate engine conditions, and uncertainty of all fluid parameters is unknown. Nonetheless, it underscores the need for engine oil filter performance to be systematically evaluated in a laboratory setting.

The benchtop facility described in this study is unique in the sense that it establishes a research-quality framework for calibrating *in situ* engine oil quality sensors and challenges their performance characteristics under a variety of conditions such as engine operating temperature and flow rate, orientation, and transient temperature spikes.

2.2 Facility Requirements

The goal of this test facility is to systematically study the performance characteristics of the OQS under controlled conditions of temperature, flow rate, and sensor spatial orientation. To this effect, the facility will duplicate the oil flow features in a typical automotive diesel engine with an inline oil filter. From a measurement standpoint, the facility shall have carefully calibrated pressure and temperature sensors and a flow meter. The facility shall have a PID-controlled heater, a gear pump for oil circulation, and a piping system rated for pressure and temperature. Since the oil is an energetic medium, safety features shall be incorporated for emergency shutdown and fire safety. Potential risks and mitigation strategies are outlined in Table 2.1.

Table 2.1 Potential benchtop facility risks and mitigation strategies.

Risk	**Mitigation Strategies**
Fire Hazard	Temperature cutoff limit on heater control of 240 °F, operation range well below flash point of about 400 °F, heater orientation prevents localized hot spots
Hydraulic Line Failure	All components designed with a factor of safety of 3 for pressure, master emergency stop, rigid connections prevent kickback
Runaway Pump	Current limits set on motor controller
Runaway Heater	Heater controller fused and possesses temperature cutoff
Harm to Personnel	PPE required during loop operation, insulated heater tank and hydraulic lines, oil containment tray

In addition, upper thresholds for operating temperature and flow rate have been established. Table 2.2 shows the chosen upper and lower bounds of operating parameters in the benchtop test facility that mirror the engine operating conditions.

Table 2.2 Engine-informed operating parameters for benchtop facility.

Parameter	**Lower Bound**	**Upper Bound**
Total Oil Volume	3.5 quarts (3.3 L)	5.5 quarts (5.2 L)
Temperature	70 °F (21 °C)	240 °F (116 °C)
Pressure	0 psig (0 kPa)	80 psig (552 kPa)
Flow Rate	2 gpm (7.6 L/min)	8 gpm (30.3 L/min)

Common automotive industry nomenclature and commercially-available industrial process components in the United States use the Imperial System of measurement, hence, for consistency, the design and operation of the facility uses this system as well.

From a precision facility design and performance standpoint, the following criteria were established. The temperature of the fluid should be controllable to ±0.6 °C (±1 °F), the pressure should be controllable to ±0.7 kPa (±0.1 psi), and the flow rate should be controllable to ±0.19 l/min (±0.05 gpm).

Standard operating procedure for the facility when changing the working oil requires draining the primary oil to 95% of the fill volume and then repeatedly flushing with the replacement oil before replacing a new filter and a new batch of replacement oil. This protocol ensures that the tested oil is not contaminated by the presence of the previous oil.

2.3 Facility Mechanical Design

A CAD model and final assembly of the calibration loop are shown in Figure 2.1.

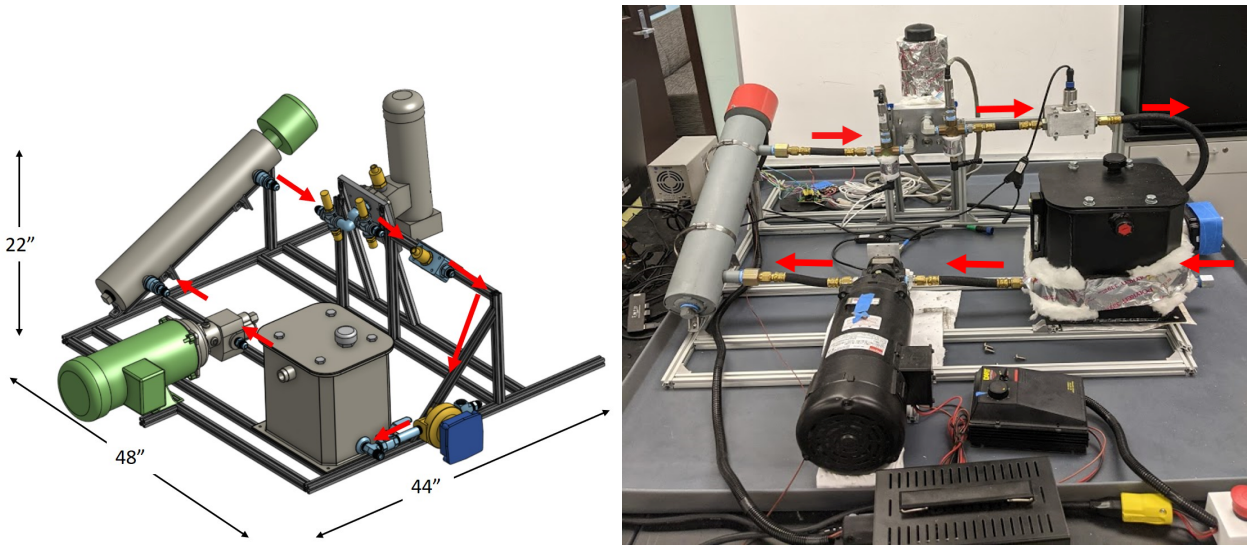

(a) CAD model. **(b)** Complete benchtop facility.

Figure 2.1 CAD and image of benchtop facility showing flow direction.

A schematic of the calibration loop and its components, using standard piping and instrumentation diagram (P&ID) symbols, is shown in Figure 2.2 and outlined in Table 2.3.

The heater temperature control unit, motor controller, interfacing circuitry between the instrumentation and data acquisition board, and the data acquisition board are not shown in Figure 2.2. The heater is placed upstream of the filter to guarantee a driving back pressure in the lines for safe heating.

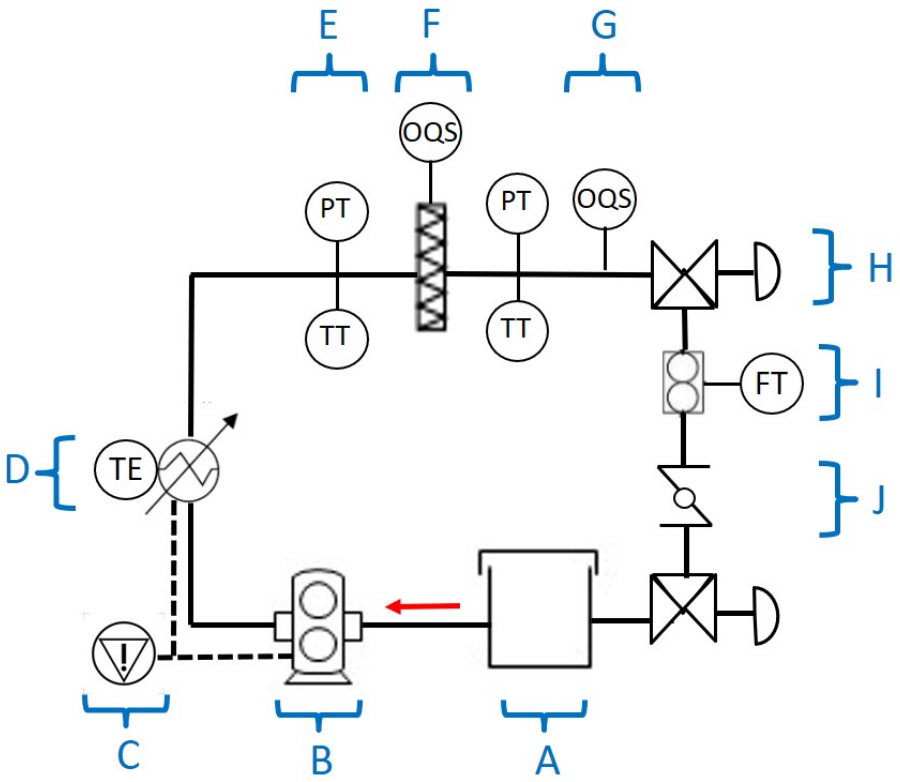

Figure 2.2 Schematic of benchtop facility.

Table 2.3 Benchtop facility component labels from Figure 2.2.

Label	**Component(s)**
A	Closed tank (vents to atmosphere, fabricated inner plates prevent air introduction)
B	Gear pump (motor-driven)
C	Emergency Stop
D	Heater with type-T thermocouple
E	Pressure transducer and Pt100 RTD
F	Oil filter housing and filter-mounted OQS
G	Adjustable inline manifold and inline OQS
H	Tee fitting with removable drain plug
I	Flow meter
J	Butterfly valve

2.3.1 Major Components

Pump

A Dayton ½″ heavy-duty rotary gear pump head was selected, as it met the maximum operating requirements of temperature, pressure, and required flow rate. It is capable of handling oil media, can operate up to 280 °F and 125 psi and is able to supply 10.5 gpm at 75 psi with 1 hp input power, with a maximum speed of 1,725 rpm. The pump head was mounted to a Dayton 1 hp, 1,750 rpm 90 V DC permanent magnet motor with fan cooling (Figure 2.3). This motor was controlled with a 120 V AC input, maximum 90 V DC and 10 A output Dart Controls DC speed controller. The internal potentiometers of this controller were adjusted for the specifications of the connected motor. The motor was securely fastened to the aluminum extrusion frame and slightly elevated as a local high point between the reservoir and heater tank for drainage purposes.

A typical gear pump is capable of supplying a constant volumetric flow rate independent of oil viscosity and is a common choice for industry, as the volumetric flow is dependent only on the rotational speed of the gears. With the flow rate monitored at all temperature set points, the chosen gear pump showed <1% flow rate slippage over the operating temperature range of 180-230 °F for a given pump speed.

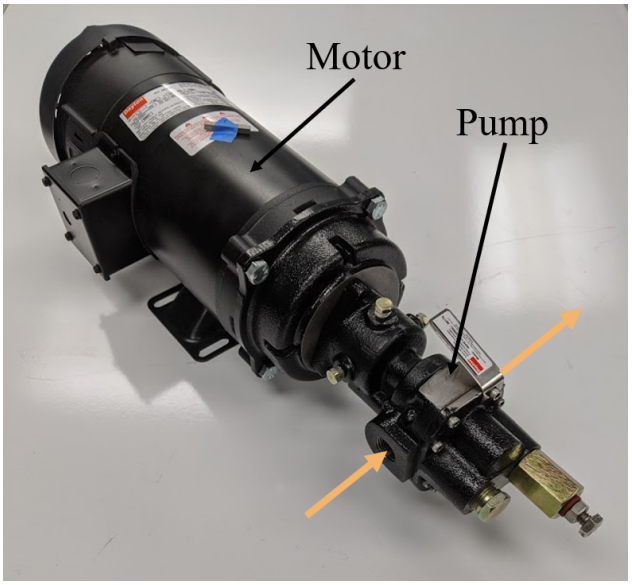

Figure 2.3 Motor and gear pump assembly.

Heater

A Watlow circulation heater, consisting of a flat bar immersion heating element within an insulated tank (Figure 2.4a), was chosen to heat the oil. Immersion heating elements were chosen over external wrap heating elements for their effectiveness and simplicity. The heating element, a Watlow FIREBAR heater, is a flat immersion heater compatible with petroleum-based fluids. The heater was chosen such that the volumetric heating to the desired operating temperature could be slow and deliberate from a safety and functional standpoint.

The flat, folded shape of the heating element (Figure 2.4b) provides a low heating power density of 15 $^{W}/_{in^2}$, preventing oil hydrocarbon oxidation, oil coking, and localized regions where oil can approach its flash point. Additionally, the heater assembly was oriented 25° from horizontal, with the inlet cold oil at the bottom and outlet hot oil at the top.

A built-in large T-type thermocouple circuit was used to measure oil temperature within the circulation heater (Figure 2.4b). This interfaced with a Tempco TCP-1000 process control console with an internal PID controller ((Figure 2.4c). After tuning the controller around a 200 °F nominal operating temperature several times, it was able to hold temperature within 1 °F with minimal overshoot.

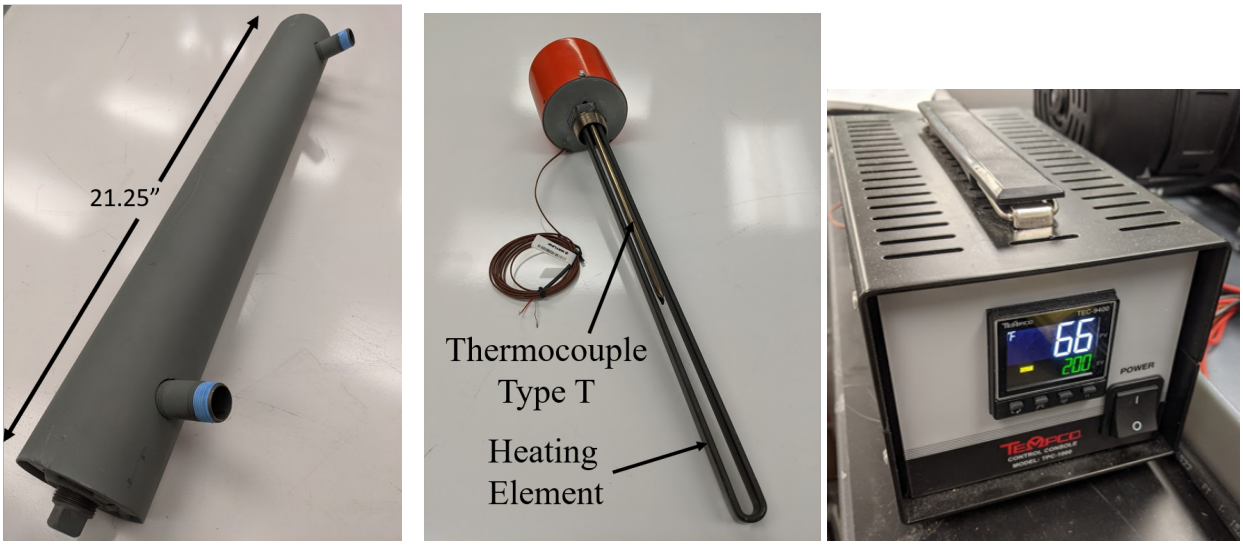

(a) Insulated heater tank . **(b)** Heating element and thermocouple. **(c)** Process control console .

Figure 2.4 Heater assembly and control console.

Filter Housing

Only one suitable location on the testbed engine oil filter housing was found for mounting the OQS for *in situ* monitoring (1.3). This location ensured that the oil measured by the OQS was in constant circulation and not a stagnant region. In this configuration, the OQS was oriented 15°with respect to vertical. Consequently, this orientation was duplicated in the benchtop facility and the OQS data was examined against an unconstrained OQS to validate the suitability of this location for measurement quality.

Figure 2.5 shows the direction of the oil flow through the filter complex; Here, the oil leaves the engine block downstream of the pump, where it passes a check valve used to keep the filter primed after shut down. It then travels down to the oil cooler, a heat exchanger with engine coolant as the cooling fluid. The oil then travels up into the filter column itself, where it is radially forced to the central axis of the filter. Figure 2.5 shows the OQS orthogonally interrupting the filtered oil in its path back into the engine block. A fabricated section of $\frac{1}{2}''$ BSPP aluminum pipe was concentrically welded around a hole drilled into the top plane of the filter housing to provide an access port for the OQS.

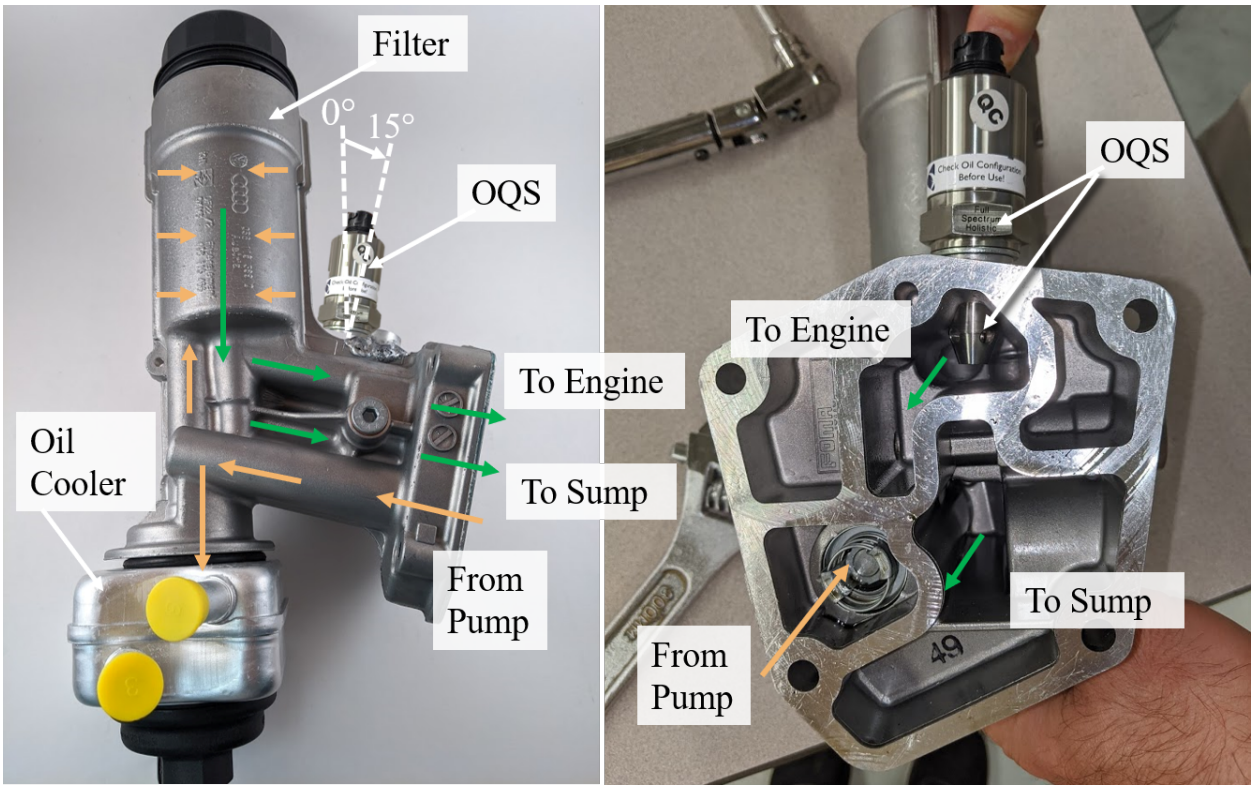

Figure 2.5 OQS location in the filter housing.

On the test facility, the filter housing unit was mounted 15° from vertical to a custom-fabricated adapter plate with matching engine hole patterns. The bottom sump drain hole was plugged, for it does not contribute to the flow in the upper cavity.

Hoses and Fittings

Parker Series 201 Hose has a nominal $^{13}/_{32}''$ inner diameter, replicating the diameter of the holes on the engine block. It is compatible with lubricating oils and has a synthetic rubber inner material and is reinforced with a steel and fiber braid, possessing a low thermal conductivity. It has a maximum operating temperature of 302 °F (150 °C and maximum operating pressure of 3000 psi (21 MPa). These hoses are semi-rigid to allow for alignment imperfections and thermal expansion without stressing the connections but also be able to maintain a constant shape during operation. Parker Series 10626 with female JIC 37° swivel fittings allow the hose to be orientation-agnostic for a leak-proof assembly.

Reservoir

Oil filling, draining, and degassing is accomplished through a vented two gallon hydraulic reservoir with a gasket-sealed cover and breather cap. Sheet metal plates were fabricated and welded within the reservoir to limit the footprint of the reservoir base (Figure 2.6) to ensure smooth flow through the reservoir and to prevent the entrainment of air.

Figure 2.6 Benchtop facility reservoir with internal modification.

OQS Manifold

An inline OQS manifold was installed downstream of the filter housing complex to house the reference OQS, which offered an opportunity to vary the orientation with respect to the gravity vector and examine the quality of data from the filter-mounted OQS (Figure 2.7). The manifold was fitted with swivel fitting adapters so that the OQS could be rotated in 45° increments from 0° (vertical with probe tip pointing down) to 180°, the assumed worst case orientation. A series of sheet metal brackets were fabricated for this purpose. The post-filter temperature and pressure measurements were representative of the fluid conditions for this OQS location (Figure 2.1b).

Insulation

Though the heater tank and hoses were thermally insulative, the large metal components caused some heat loss observed during preliminary testing. Fiberglass insulation was therefore wrapped around the oil filter housing, reservoir, and cross fittings of the temperature sensors. This ensured that there was minimal heat loss across the filter housing assembly.

Figure 2.7 Tan Delta inline OQS manifold.

2.3.2 Safety

Oil leaks or spills, especially if they occur at the operational high temperatures and pressures, can cause significant harm to personnel and damage to the equipment and laboratory. Therefore, facility safety was of utmost importance when designing the test loop.

As detailed above, all components are rated well above the proposed temperature. All components and fittings were designed with a structural factor of safety of at least 3. All mechanical seals were Viton, assured up to a sustained 205 °C, and all pipe threads used hydraulic PTFE sealant tape. To contain any potential spills, a thick plastic tray with 2" sidewalls was placed under the entire loop. Also, fire extinguishers, oil absorbent granules, and oil absorbent pads were easily accessible. All personnel were required to wear eye protection when using the test loop and have a partner on standby. In the event of abnormal operating conditions, an emergency stop button was installed in a rapid prototyped enclosure near the loop to cut power to the pump motor and heater. All wires were rated to at least twice the expected current draw and wrapped in plastic sheathing to protect against any wear on the insulation.

The frame was constructed of 20 mm x 20 mm aluminum extrusion to securely fasten all components of the facility and provide modularity for any future change outs in the post-heater test section.

2.4 Facility Instrumentation

2.4.1 Major Components

Pressure Transducers

The oil filter housing complex instrumentation suite is shown in Figure 2.8, with pressure and temperature sensors located immediately upstream and downstream of the filter housing complex.

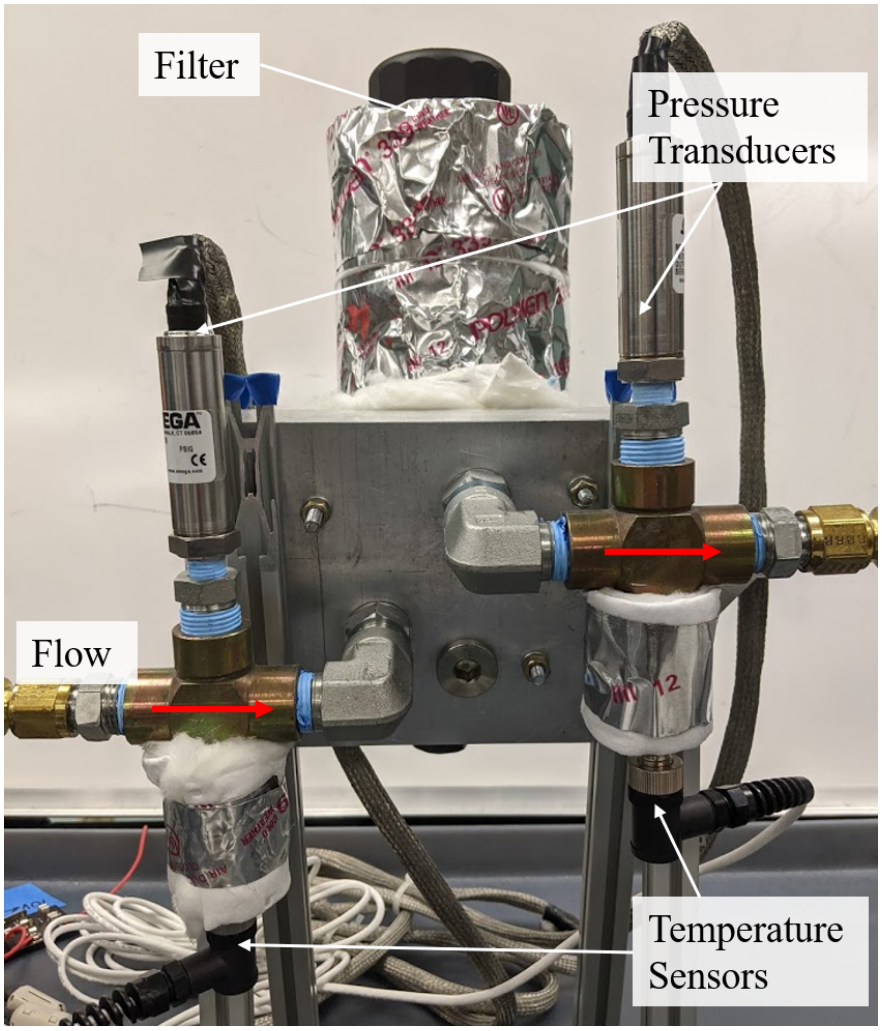

Figure 2.8 Insulated oil filter housing complex with associated instrumentation.

The chosen pressure transducers are from the piezoresistive Omega PX409 series, which uses a strain bridge that is deformed through a sealed stainless steel diaphragm. It

was configured to measure gauge pressure from 0-50 psi with a ratiometric 0-5 V DC output and accuracy of ±0.08% including linearity, hysteresis, and repeatability. This transducer can operate up to 240 °F. The transducer has a burst pressure of 400 psi, ensuring its protection against any potential hydraulic shock. The sensor has a $^1/_4''$ NPT male pressure port connection, and its stainless steel wetted parts are compatible with lubricating oil media.

Each transducer came with a 5-point NIST traceable calibration certificate to verify its performance. The pressure sensors were installed in cross fittings before and after the oil filter housing, with adapters ensuring that the probe tips were recessed out of the flow so as not to interrupt the flow and only measure the static component of the pressure.

Each sensor cable came with a foil sheath, that attenuates high frequency (above 15 kHz) noise, that was connected to the circuit common ground, and the cable was tied so that it would not form inductive loops. To attenuate the observed electromagnetic interference (EMI) 60 Hz noise, tinned copper wire braid was sleeved over the length of the cable and grounded on the sensor housing. Ferrite cores were also placed at the ends of the cable. This reduced the peak-to-peak oscillations of the noise to about 5 mv (0.05 psi). Another observed frequency was between 5 and 20 Hz and was not attenuated by the additional EMI shielding, indicating that it was due to pressure pulses from the pump. This was confirmed by motor speed calculations. These oscillations still were to within 0.05 psi, however. Pressure snubbers could potentially further dampen the measured pulsations.

Temperature Sensors

Omega Compact Pt100 RTD sensors were selected for inline temperature measurement. These stainless steel sensors operate from -50 to 120 °C (-58 to 248 °F) with a response time of less than five seconds and can withstand up to 580 psi. These sensors are IEC 751 class A rated, with a temperature resolution of ±0.31 °C at 80 °°C, ±0.35 °C at 100 °C, and ±0.39 °C at 120 °C. The sensors are four-wire type, where the measured voltage is across two leads that do not carry the power current, eliminating the effects of false high readings due to lead resistance. The resistance of these sensors decreases 0.385 $^{\Omega}/_{^{\circ}C}$.

Each sensor was provided with calibration data for its resistance at 0 °C. To determine the resistance, the Pt100 was wired to the high side of a voltage divider circuit with a highly stable MR106 Vishay wirewound 993 Ω resistor. The two measuring wires of the Pt100 had a 0.1 μF capacitor connected in parallel to reduce noise.

To calibrate the sensors, a controlled water bath was set to various temperatures

near engine oil operating temperature and allowed to assume steady state conditions (Figure 2.9). Data from two precise digital thermometers with a determined ±0.1 °C accuracy was recorded and averaged as the truth value with simultaneous Pt100 measurements. This data was used to form a best fit linear correction equation with a 95% confidence interval for each sensor to be used in post-processing (Figure 2.10). The calibration equations for the pre-filter and post-filter Pt100 sensors are given in Equation 2.1 and Equation 2.2, respectively. The temperature sensors were insulated on the benchtop facility to prevent thermal losses through their extended ports on the cross fittings.

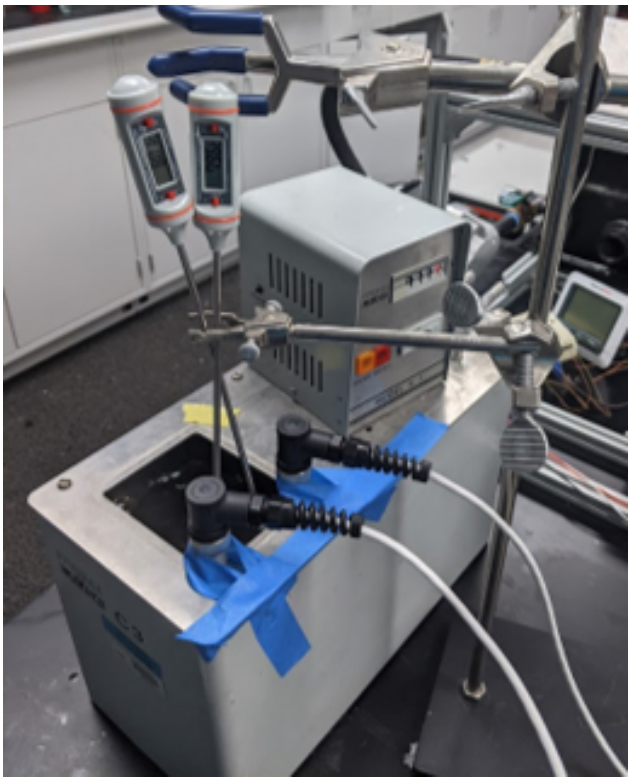

Figure 2.9 Controlled water bath for calibration of Pt100 temperature sensors.

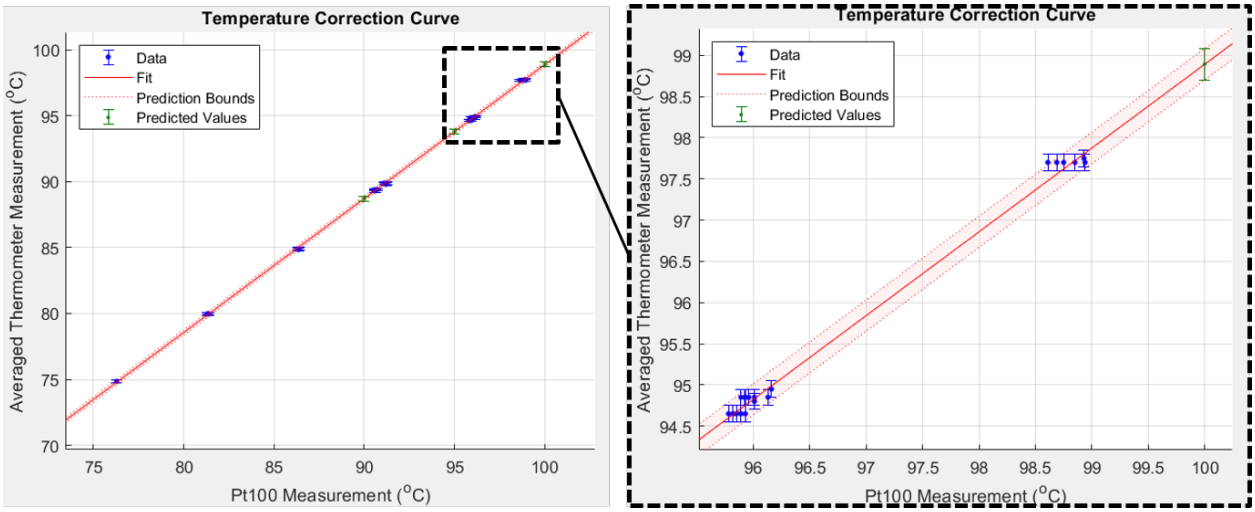

Figure 2.10 Calibration curve for the pre-filter Pt100 sensor.

$$T_{corr} = (1.107)T_{meas} - 2.775(^{\circ}C) \tag{2.1}$$

$$T_{corr} = (1.010)T_{meas} - 1.749(^{\circ}C) \tag{2.2}$$

Oil Quality Sensor

A Tan Delta Systems OQSx-GenII oil quality sensor was chosen to measure the oil loss factor for the testbed engine. A basic schematic of the OQS in Figure 2.11 shows its cylindrical capacitor sensing tip with portholes to limit flow rate effects and prevent debris accumulation. Embedded electronics in the sensor body are used to compute the loss factor and also correct for loss factor temperature dependence through an onboard temperature sensor. Tan Delta Systems provides a database of life cycle profiles for various oils, and the sensor was configured for the oil type used in the test loop.

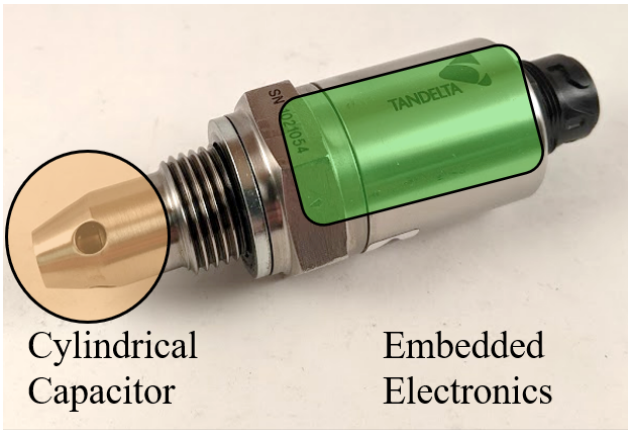

Figure 2.11 Basic schematic of the Tan Delta OQSx-GenII.

Flow Meter

A Flomec oval gear flow meter was selected to measure the flow before it reenters the reservoir. An oval gear flow meter operates similarly to the gear pump, where a constant volume of fluid is allowed through the gears with each revolution. The rotational speed of the gears, measured as pulses from a Hall effect sensor, can then be compared to the factory calibration values to determine volume flow rate from the resulting square wave-like output (Appendix B). This flow meter is able to operate up to 250 °F and 580 psi and can measure flow rates from 0.26 to 10.6 gpm. The flow meter was oriented such that the sides of the gears would not rest on the housing. A pressure regulation butterfly valve was placed downstream of the flow meter.

The flow meter uses a pulsed Reed switch to calculate flow rate for an attached digital display. However, the test loop data acquisition circuit uses the pulsed Hall effect output to calculate the flow rate, using the meter's calibration value of 640.115 pulses/gallon. Measurements showed an uncertainty value of ±0.06 gpm.

2.4.2 Data Acquistion Components

Cables and Noise

As stated, the motor and high current carrying wires generate EMI, and the sensitive pressure transducer cables were protected as described. All other instrumentation wires were made as twisted pairs to negate crosstalk and mitigate the effects of EMI. All wires were made

with header pin connectors for easy connection and change out with the circuit board and DAQ board.

Power Supply

A KORAD KD3005D DC linear regulated power supply was used to power the instrumentation. This lab grade power supply allows for a constant voltage with noise rejection and < 1 mV rms ripple.

Data Acquisition Board

A National Instruments USB-6212 was chosen to interface with the instrumentation to collect data. The BNC analog inputs can sample up to 400 kS/s with a common mode rejection ratio from DC to 60 Hz of 100 dB and have an input impedance of $>$10 GΩ and an input bias current of $\pm$100 pA. With a $\pm$5 V input range chosen, the 16-bit ADC has a resolution of about 0.15 mV. All analog inputs, configured as either differential or single-ended depending on the measurement, were referenced to a common ground connected to the circuit board and power supply. Appendix A outlines the data acquisition and processing software.

Instrumentation Circuit Board

All of the instrumentation interfaced with a custom-soldered compact circuit board that allowed for easy connection and disconnection for all components using screw terminals and pin connectors (Figure 2.12). A LM340AT voltage regulator and 0.2 μF capacitor ensured that the temperature sensors and flow meter were supplied with a constant voltage. The flow meter output line was connected to a step down 1 kΩ resistor. A circuit diagram is provided in Figure 2.13.

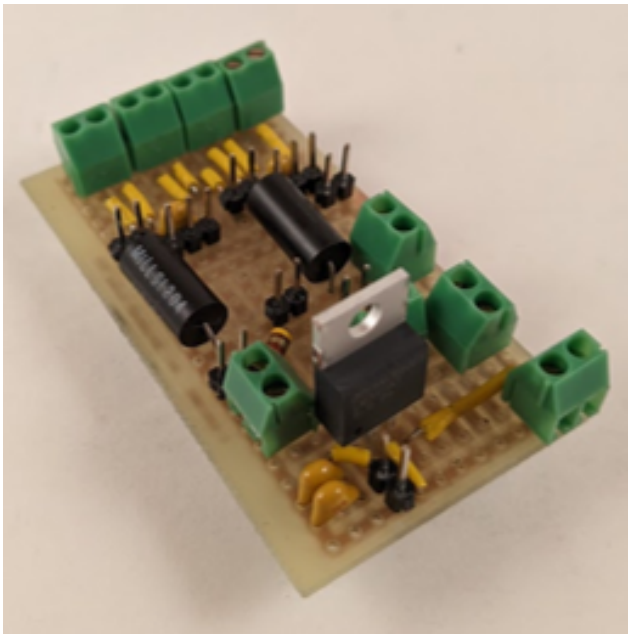

Figure 2.12 Instrumentation interface circuit board.

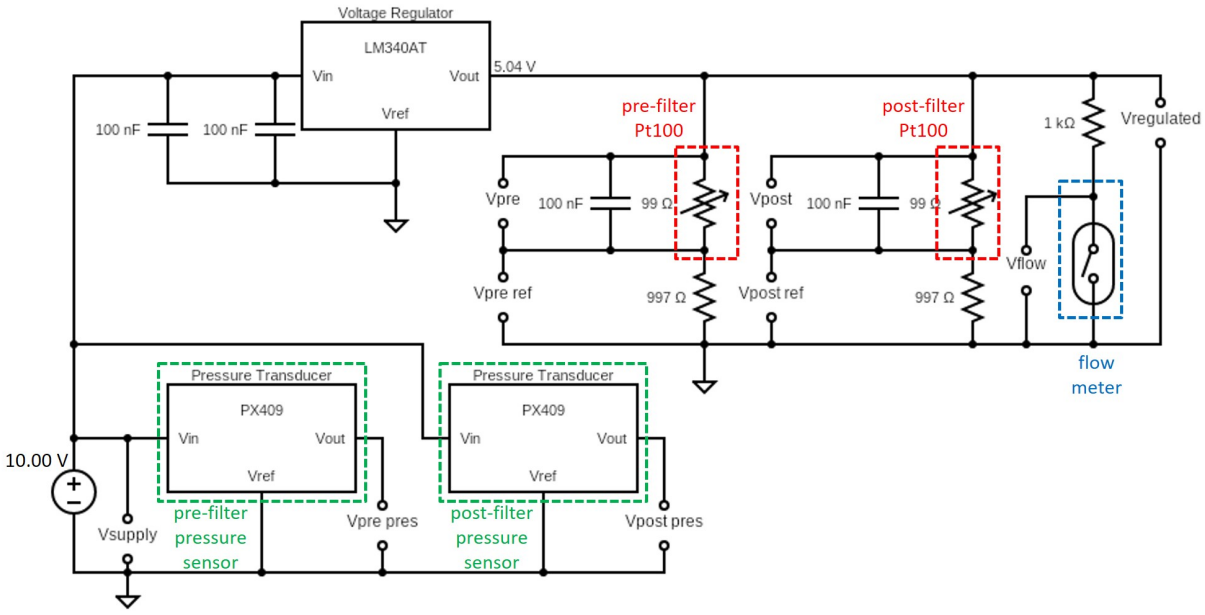

Figure 2.13 Instrumentation interface circuit board diagram.

2.5 Facility Performance

2.5.1 Operational Window

Two different oils formulated for diesel engines have been characterized in this facility. The first is a brand new semi-synthetic oil, Ravenol HPS 5W-30, the same type used in the Vollkswagen testbed diesel engine. This virgin oil was used to verify the operation of the facility and fine tune the controls and instrumentation. It was also used to evaluate a baseline OQS response for a virgin oil.

The second one used was Shell Rotella T6 5W-40, a fully synthetic oil. This oil was chosen because of access to an already degraded sample in a Volkswagen car fitted with the same diesel engine as the testbed. Oil degradation in a diesel engine, especially for synthetic blends, requires hundreds of hours of operation for measurable effects. A gallon of used oil was extracted from this Volkswagen vehicle after 8,300 miles of operation. Synthetic oils normally provide 15,000 miles of lifespan before end-of-life degradation (about 30% loss factor).

The functional operational window of the facility has been delineated in Figure 2.14; this was established through a combination of measurements and visual inspection. The maximum operating temperature is 240 °F, which is established based on the temperature limits of the pump, flow meter, and sensors. The minimum operating temperature is 90 °F and represents the lowest temperature that can be steadily maintained in the loop.

The other operational boundaries of this window are determined by the maximum pumping capability and the ability to excavate the dissolved or trapped air in the oil so that it is not continuously circulated in the loop. The lower boundary of flow rate is dictated by the requirement to establish a thermally uniform flow.

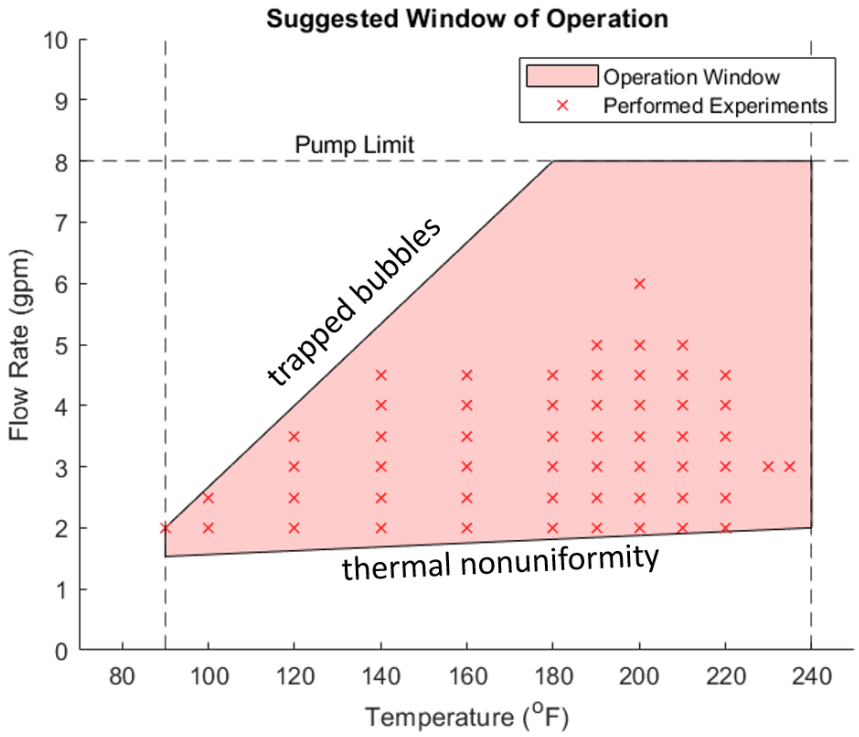

Figure 2.14 Window of operation for the benchtop facility.

The diagonal line in Figure 2.14 represents the demarcation between a flow with trapped air bubbles and a clean flow. This was established through visual inspection of flow quality in the reservoir (Figure 2.15). There should be no observable trapped air in the oil. At higher temperatures, the lower viscosity of the oil allows buoyant air bubbles to easily escape from the fluid. Higher flow rates trap the air bubbles and keep them circulating in the flow. Figure 2.15a shows the normal operation within the window, and Figure 2.15b shows abnormal operation with trapped bubbles.

(a) Operating temperature. **(b)** Low oil temperature.

Figure 2.15 Air entrapment in reservoir at operating temperatures and at low temperatures.

2.5.2 Temperature Control

The temperature of the facility is programmable to 1 °F with a maximum error in steady-state tracking of ±0.5 °F (Figure 2.16). When increasing the temperature setpoint within the operating temperature range, there was some observed overshoot due to the system being thermally underdamped, but it was limited to only 1 °F. To achieve this optimal performance, the heater was tuned multiple times at 200 °F and 3.0 gpm flow rate; these are median parameters of facility operation informed by engine operation. It was noted that the heater thermocouple that controls the oil temperature in the heater tank consistently read about 2-3 °F higher than the calibrated Pt100 RTDs. This likely represents thermal losses in the line and requires an offset when programming the setpoint temperature.

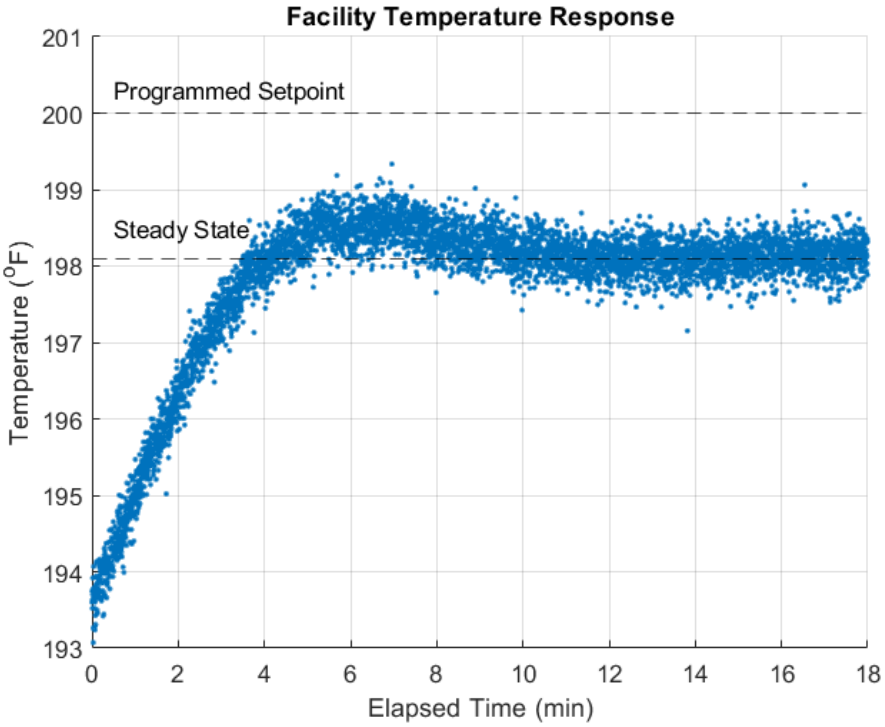

Figure 2.16 Steady state tracking of the benchtop facility temperature.

The transient temperature response of the facility is shown in Figure 2.17. The settling time to warm the oil from 70 °F to 200 °F is about 45 minutes at 3.0 gpm, and the settling time to warm the oil 20 °F within operating temperatures is about 15 minutes.

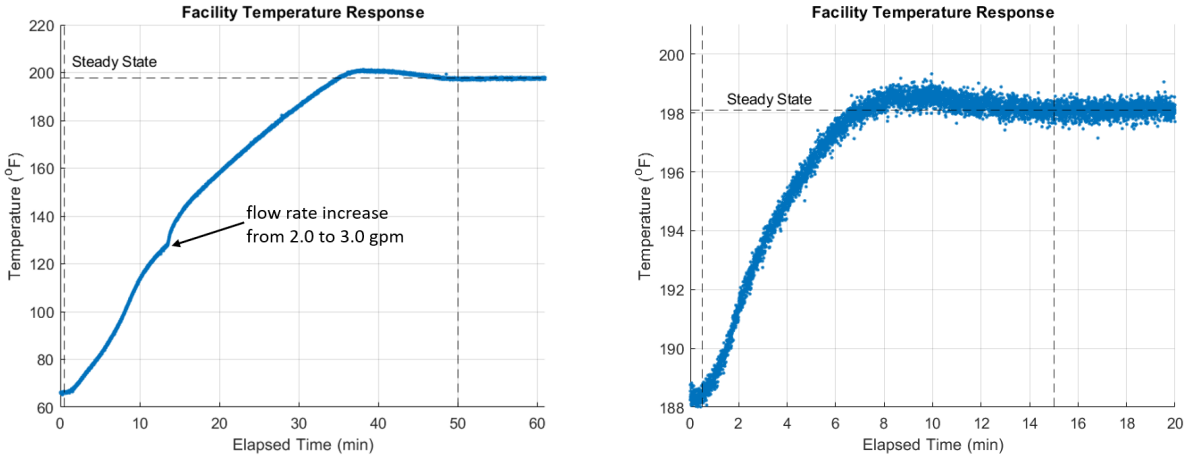

(a) Room temperature to operating temperature. **(b)** 20 °F increase at operating temperature.

Figure 2.17 Transient temperature response of the facility.

The steady-state operating temperature at the oil filter housing complex test section demonstrated a maximum measurement uncertainty of ±0.65 °F, comparable to the stated accuracy of the temperature sensors (Figure 2.18) with no observable drift. The heat loss through the oil filter housing complex was minimized through the use of fiberglass insulation. The average temperature discrepancy between the pre-filter and post-filter sensors was 0.2 °F, with the post-filter sensor measuring the higher temperature. This is most likely due to measurement uncertainty corresponding to each sensor. If it assumed that all frictional pressure loss becomes heat and that the oil filter housing complex is adiabatic, then using measured pressure values, calculated density values ρ and a general specific heat c_p of 2180 $^{J}/_{kgK}$ for the oil, the temperature increase would be expected to be only 0.05 °F across the filter (Equation 2.4).

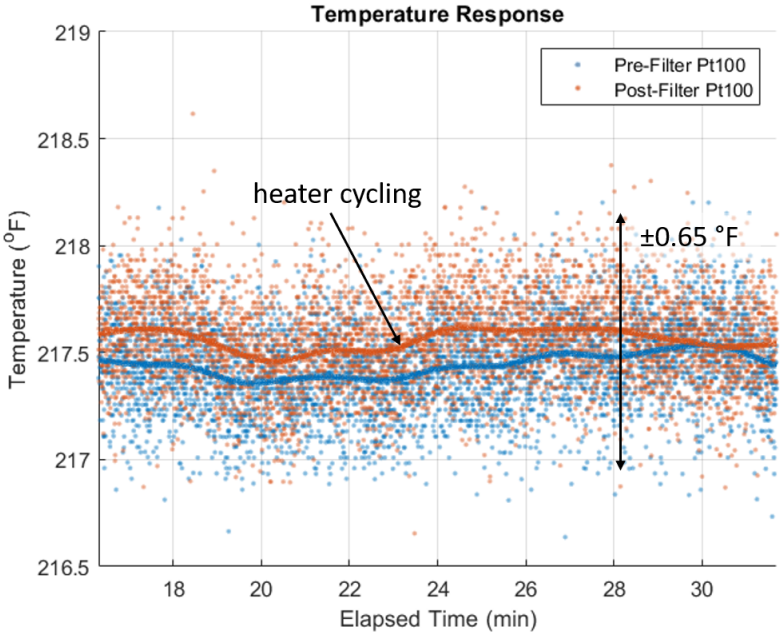

Figure 2.18 Steady state temperature measurement across the oil filter housing complex.

$$\rho c_p \Delta T = f\frac{\rho V^2}{2} = \Delta p \tag{2.3}$$

$$\Delta T = \frac{\Delta p}{\rho c_p} = \frac{48780Pa}{796\frac{kg}{m^3}2180^{J}/_{kgK}} = 0.03°C \quad (0.05°F) \tag{2.4}$$

CHAPTER THREE

EVALUATION OF OIL QUALITY

3.1 Filter Characterization

The performance of the mechanical oil filter in the benchtop facility is dependent on the condition of the circulating oil and the working condition of the filter. It is a useful tool to evaluate the overall performance of the benchtop facility. A new oil filter was used whenever an oil was placed in the facility, regardless of its state of degradation. The majority of the pressure drop across the oil filter housing complex occurs across the oil filter and is measured by the pressure sensors located just upstream and downstream of the complex (Figure 2.8).

Oil enters the cylindrical filter housing in the outer perimeter and moves radially inwards through the filter (Figure 3.1b). The filter used in this facility corresponds to the one recommended for the testbed diesel engine (Figure 3.1a). The filter material is primarily composed of cellulose, with small pores between fibers to allow oil passage. The filter is pleated to increase the surface area of filtration and improve flow throughput. Over time, pores in the filter become clogged by the filtered contaminants, and the filter's permeability decreases. Throughout its effective life, the bulk flow through the filter can be characterized as viscous flow.

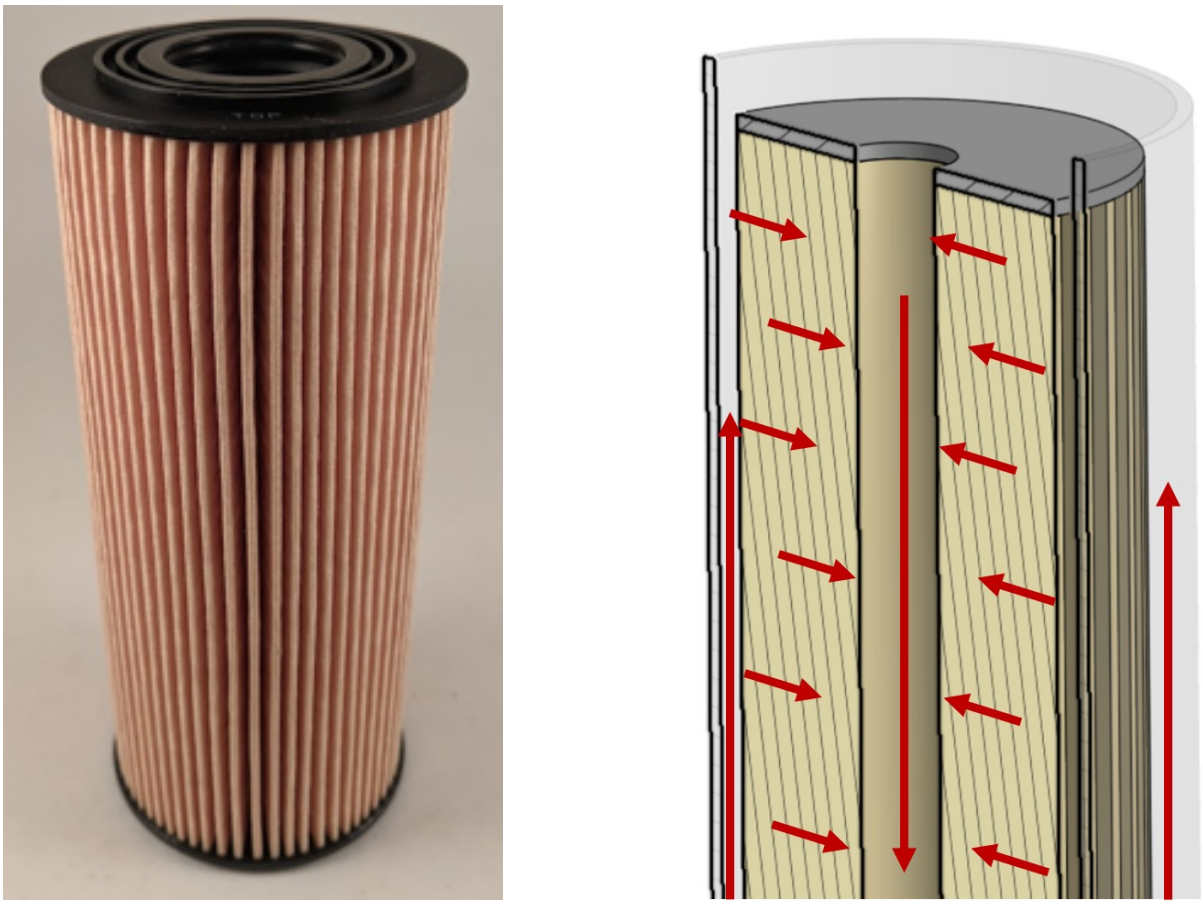

(a) R84210 pleated filter. **(b)** Oil flow through filter.

Figure 3.1 Testbed diesel engine and benchtop facility oil filter and flow schematic.

Figure 3.2 shows the measured pressure drop across the oil filter complex as a function of flow rate for the virgin oil (Ravenol HPS 5W-30). There is a ± 0.05 psi and ± 0.04 gpm measurement uncertainty for the pressure and flow rate measurements, respectively, as shown in the inset of Figure 3.2. These uncertainties are due to a combination of the pressure sensor uncertainty and flow pressure pulsations emanating from the pump that are not entirely damped out in the large volume of the heater tank. For this experiment, 2 minutes of steady state data was collected at flow rates of 2.0, 2.5, 3.0, 3.5, and 4.0 gpm and at temperatures of 190 °F, 200 °F, and 210 °F, which are typical operating conditions for engine oil. In the operating temperature regime, the pressure drop shows a linear dependence on flow rate. The inset in Figure 3.2 points to an apparent decrease in pressure drop with an increase in temperature.

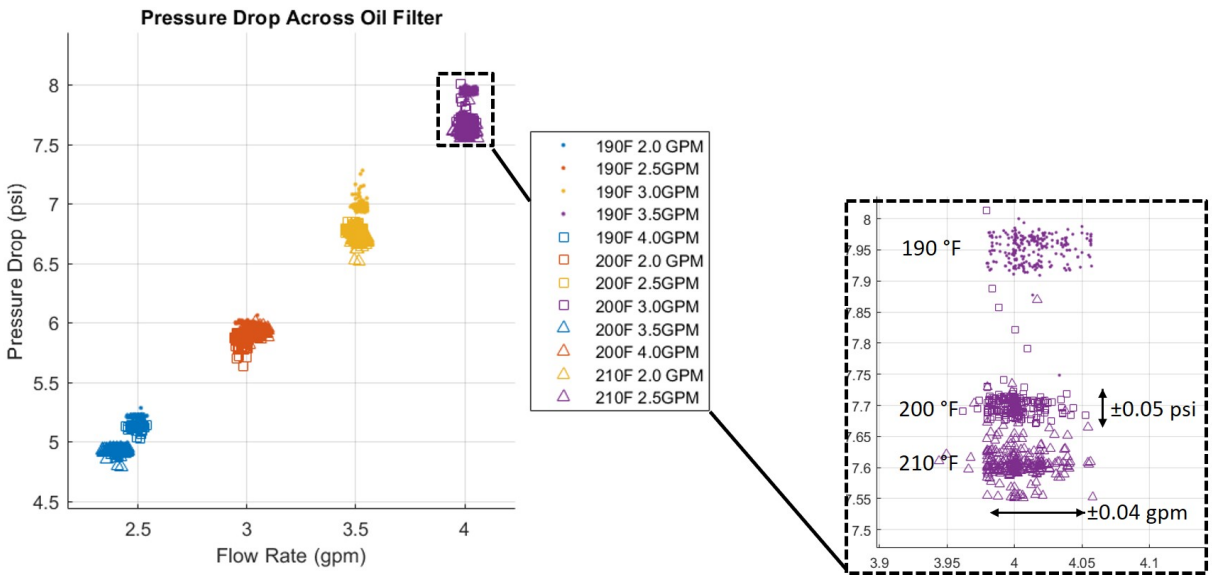

Figure 3.2 Pressure drop across the oil filter housing complex and associated measurement uncertainties for the virgin Ravenol HPS 5W-30.

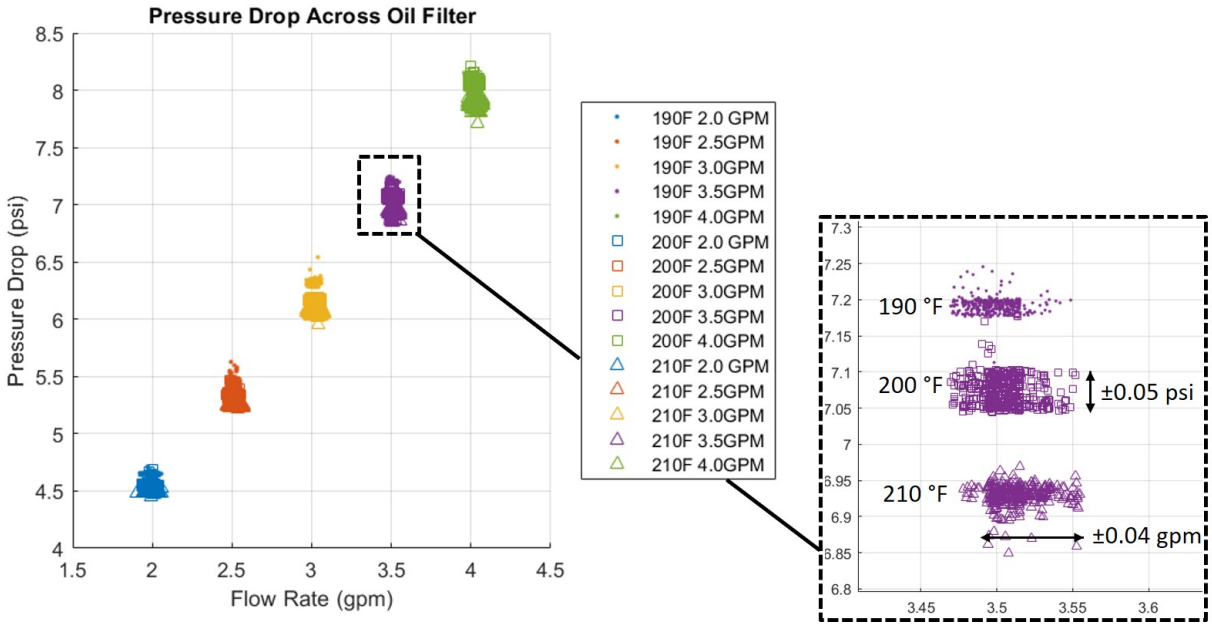

Figure 3.3 Pressure drop across the oil filter housing complex and associated measurement uncertainties for the degraded Shell Rotella T6 5W-40.

These temperature-based differences are even clearer for the degraded Shell Rotella T6 5W-40 engine oil (Figure 3.3), as these experiments were conducted after the facility went through additional examination of heat loss and incorporation of thermal insulation.

3.2 Fluid Dynamics Analysis Flow Through the Filter Complex

The filter housing complex can be examined as a major flow obstruction and the resistance to the flow through it can be simply analyzed through techniques of dimensional analysis. The pressure drop across the filter complex Δp can be characterized as a function of fluid density ρ, dynamic viscosity μ, flow velocity V, and a characteristic length scale in the piping system as shown in Equation 3.1. The most prominent flow components are the hydraulic hoses, and thereby the average diameter D of the hose has been chosen as the representative length scale, which automatically scales the fluid flow velocity. This approach to flow analysis looks at the filter as a black box, and thereby permeability variations, if any, are only captured through measured variations in the pressure drop.

The average inner diameter of the hoses was measured to be 0.423 inches. Flow velocity was calculated using the cross-sectional area and measured flow rate.

$$\Delta p = F(\rho, \mu, V, D) \tag{3.1}$$

The density and viscosity of the tested oils were computed using the equations presented in Section 1.3 and the standard values from the oil datasheets. These values are shown in Figure 3.4. The corresponding values of the degraded oil were interpreted from the datasheet values of a clean oil, as such measurement techniques are not independently made in the facility.

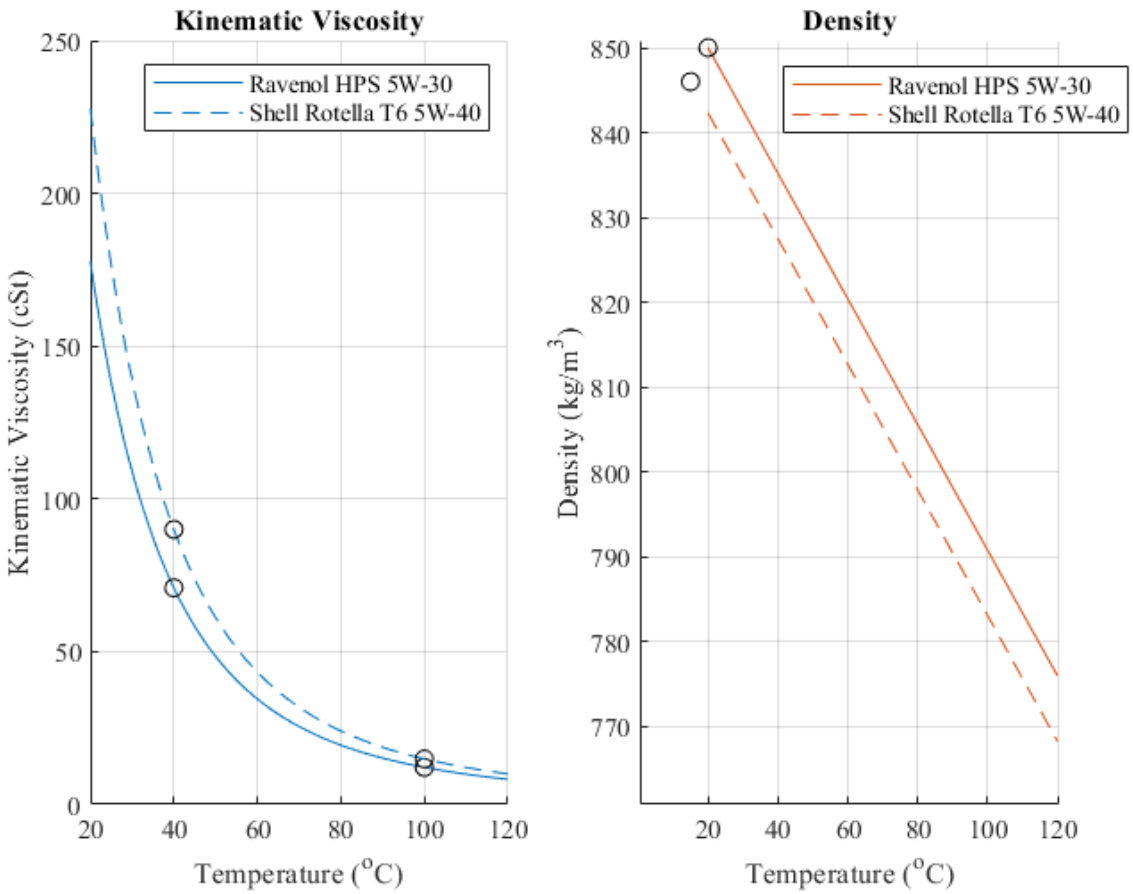

Figure 3.4 Kinematic viscosity and density for virgin Ravenol HPS 5W-30 and clean Shell Rotella T6 5W-40.

Equation 3.2 is the nondimensionalized form of Equation 3.1, where K is the friction factor for the flow across the filter complex. It is assumed that there is no pressure difference due to height, as the inlet and outlet measurement ports are of negligible height difference. The Reynold's number in this analysis was calculated using kinematic viscosity, as this value is directly computed from the Walther equation of Equation 1.1.

$$K = \frac{\Delta p}{\frac{1}{2}\rho V^2} = \phi(\frac{\rho V D}{\mu}) = \phi(\frac{V D}{\nu}) = \phi(Re) \tag{3.2}$$

Figure 3.5 shows the variation of the friction factor as a function of Reynold's number on a log-log plot, which is a typical convention for pipe flows. A classical Reynold's number dependence representative of fully developed laminar pipe flow is captured here.

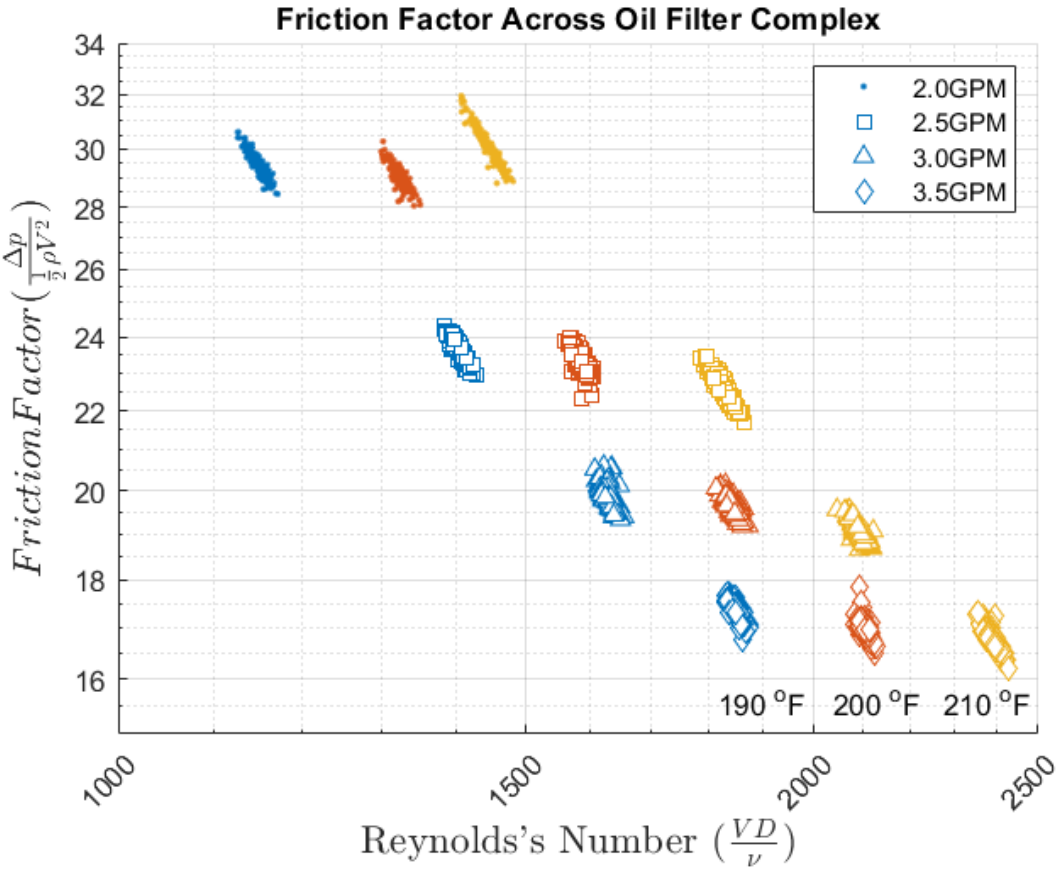

Figure 3.5 Filter housing complex friction factor data for the virgin Ravenol HPS 5W-30.

Using this approach, the slopes of the pressure drop curves n were determined as follows:

$$K = \frac{B}{Re^n} \tag{3.3}$$

$$log(K) = -nlog(Re) + log(B) = -nlog(Re) + C \tag{3.4}$$

In traditional fully developed laminar pipe flow, $n = 1$ and $C = log(64) = 1.81$. In the present context, for each steady state operating temperature, the data demonstrated that $n = 1.15$, with a 1.5% variability, and C showing a temperature dependence, where T^* is a temperature scaling factor (Equation 3.5).

$$log(K) = -1.15log(Re) + C(T^*) \tag{3.5}$$

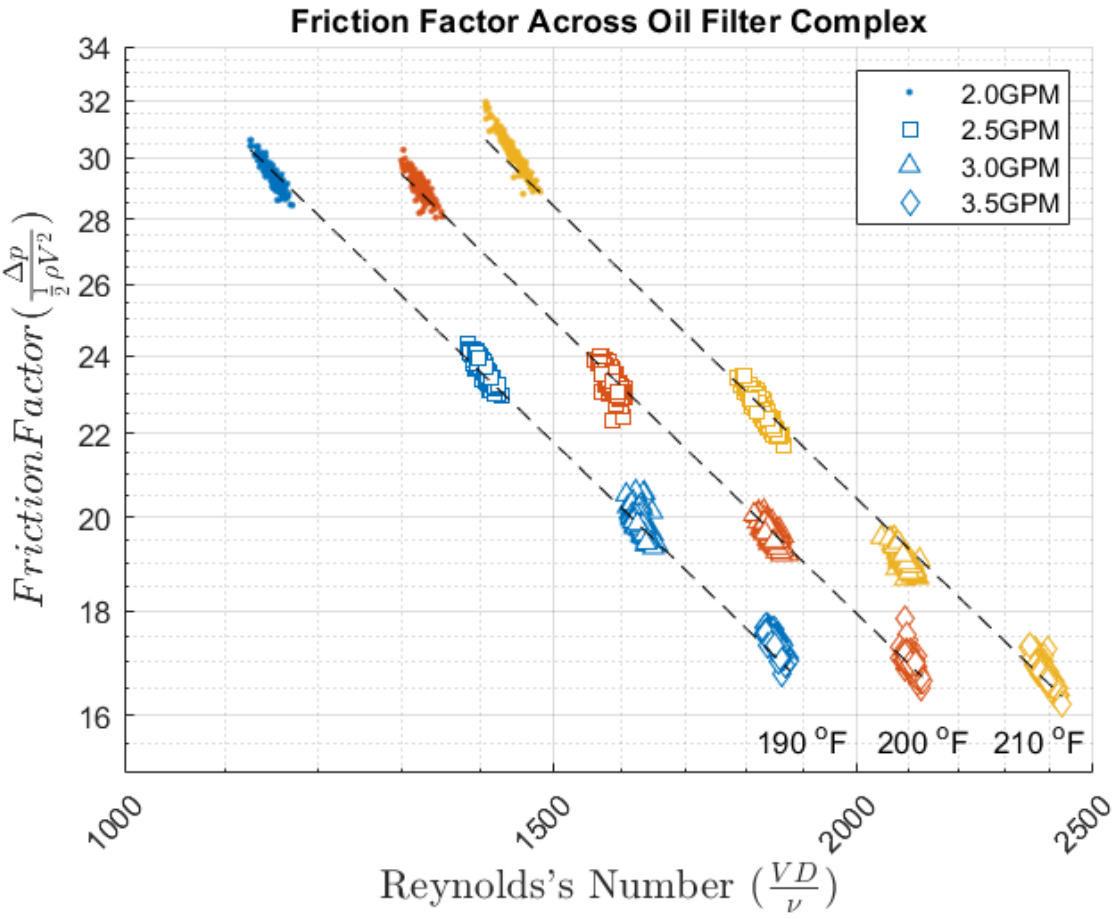

Figure 3.6 Filter housing complex friction factor data and developed equation for the virgin Ravenol HPS 5W-30.

A similar experiment was performed for clean Shell Rotella T6 5W-40 engine oil in which data was recorded for various steady-state flow rates and temperatures. Figure 3.7, shows a similar temperature dependence as that of Figure 3.6. The slope n of the linear fits for both clean oils is $n = 1.15$.

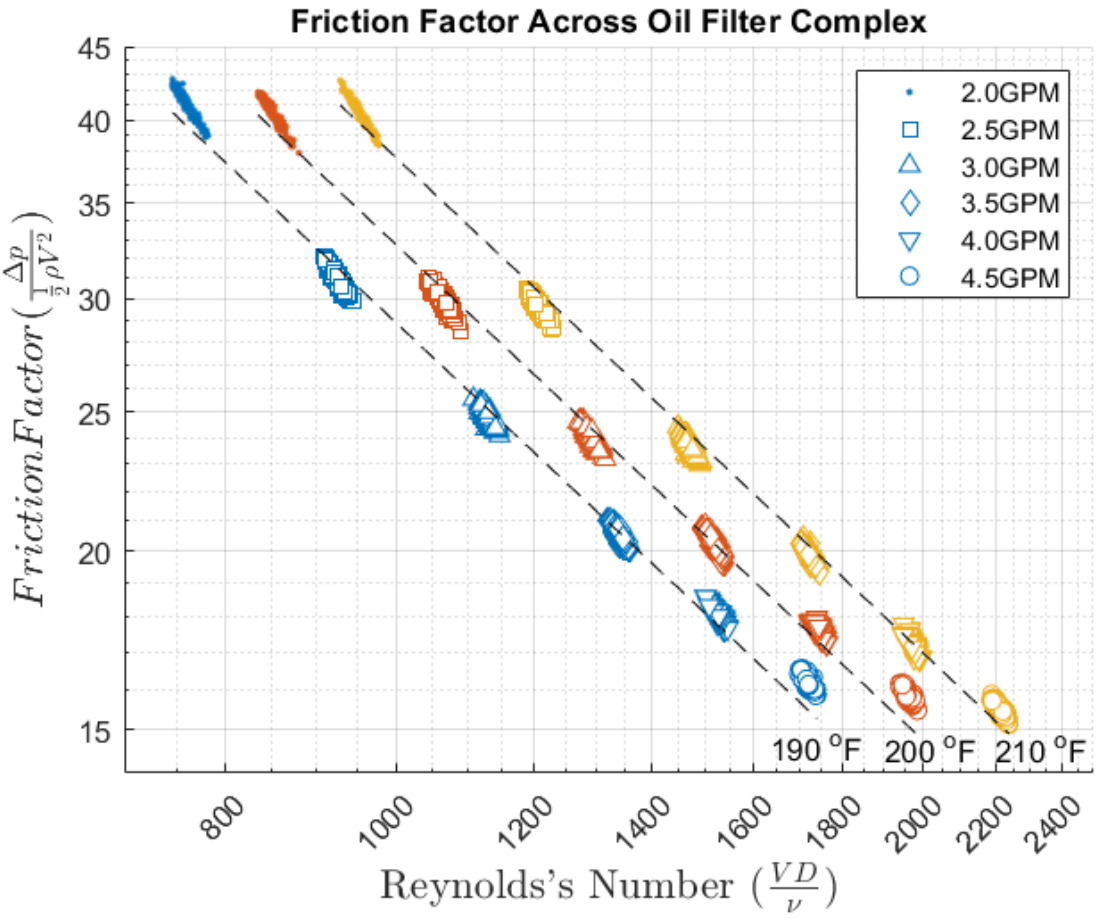

Figure 3.7 Filter housing complex friction factor data and developed equation for the clean Shell Rotella T6 5W-40.

Observation of Figure 3.6 and Figure 3.7 brought into question the possibility of a flow measurement error contributing to a lack of universal fit despite experiments being conducted at constant working fluid temperatures and with clean oils. As a first step, it was examined whether thermal transport, as in thermal diffusivity (Prandtl number), had a role when compared to momentum transport (Reynold's number). On careful examination, no correlation could be found that could explain a role for thermal diffusivity in increasing the frictional resistance across the filter complex when compared with momentum diffusivity, especially since these oils are high Prandtl number liquids.

In the next step, it was examined whether inaccuracies in flow meter measurements within the operating temperature range were contributing to this apparent anomaly. This suspicion was resolved after careful examination of the oval gears and internal surfaces in the flow meter showed no observable cause. Additionally, precision calibration data provided

by the flow meter manufacturer settled any concerns related to metering high temperature fluids (Appendix B).

Consequently, a new thought experiment was conducted with a clean oil (Shell Rotella T6 5W-40) and filter where the pressure drop experiments were conducted at constant temperatures as follows. Starting at a working oil temperature of 140 °F, the experiments were sequentially conducted with the temperature raised in steps of 20 °F to a maximum of 220 °F (Figure 3.8). Figure 3.9 shows the results when the experiments were conducted in the reverse order, with temperature decreasing in steps of 20 °F from 220 °F to 140 °F. From these two studies, it is clear that the oil filter friction factor returns to its original value, showing no hysteresis that could be resulting from filter clogging and contamination. This is highlighted by the friction factor value of 25 at a Reynold's number of 1000 for both runs.

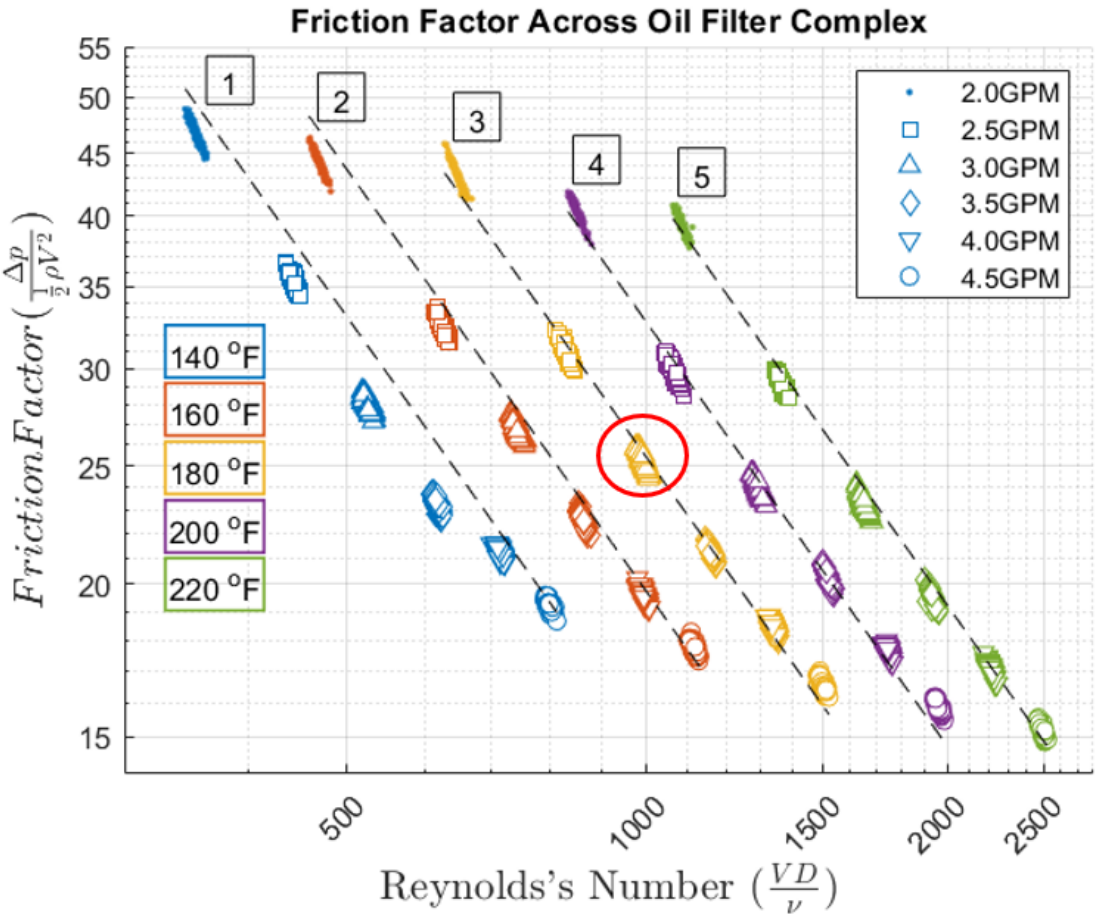

Figure 3.8 Filter friction factor hysteresis study with runs of increasing temperature.

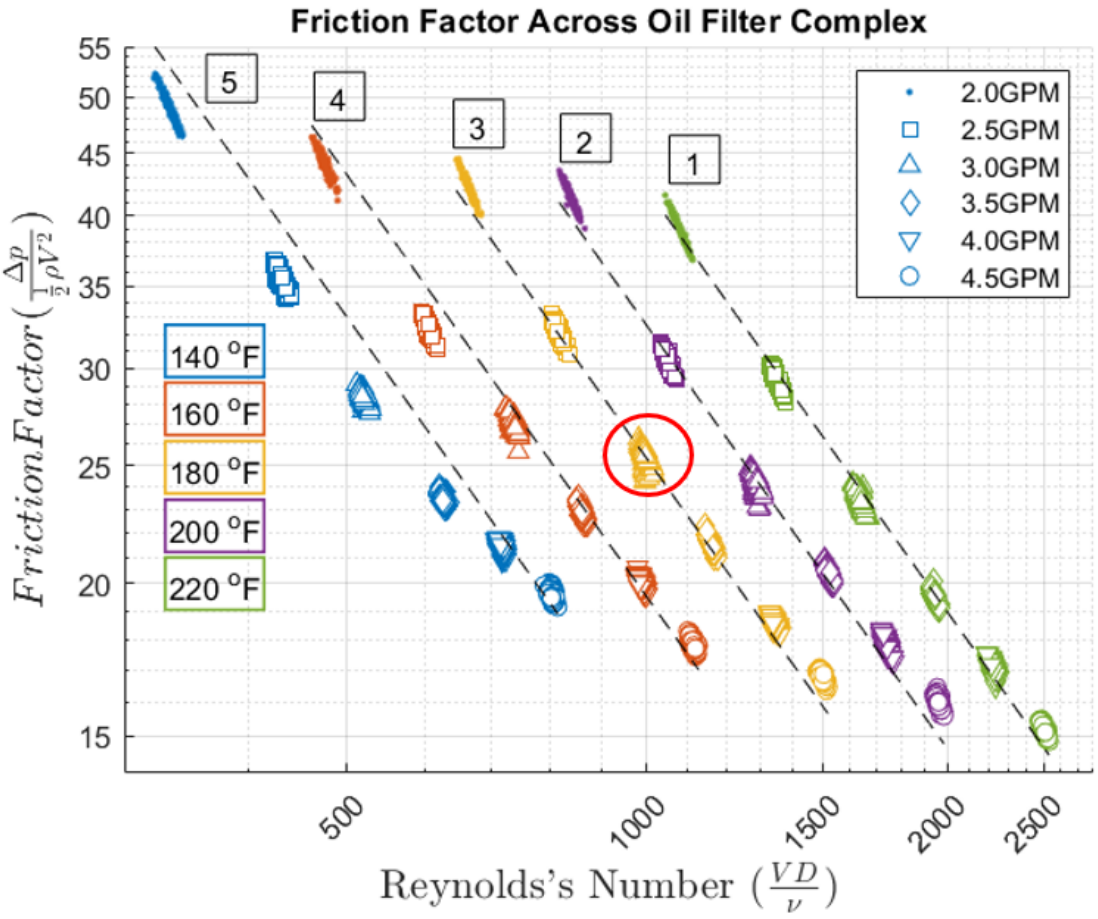

Figure 3.9 Filter friction factor hysteresis study with runs of decreasing temperature.

Observations in Figure 3.8 and Figure 3.9 point to internal changes in the resistance to fluid flow as a function of temperature, as there are no changes external to the filter complex. In the constrained volume of the filter housing, the thermal response of the filter material is possibly leading to a change in local porosity and thereby the overall permeability and resistance to fluid flow. Permeability represents how efficiently the oil can travel through the filter material and is essentially a measure of the overall resistance encountered. In this context, there is decrease in permeability with temperature increase, pointing to a decrease in porosity.

The friction factor can still represent this effect through a modification of Equation 3.5, where C captures the permeability effects of temperature. Equation 3.6 shows this, where T_0 is a reference temperature chosen as 197.9 °F from the nominal 200 °F setpoint, representative of engine operating temperatures, C_0 is the corresponding value, and D is

an experimentally-determined constant. The dashed lines in the friction factor figures are plotted with this equation.

$$C = C_0 + D(\frac{T - T_0}{T_0}) \tag{3.6}$$

Figure 3.10 shows the percentage change in permeability with an increase in temperature. This figure captures the decrease in permeability as temperature increases. In the current context of the clean oil experiments, for a 80 °F temperature increase, the permeability decreases by about 10%.

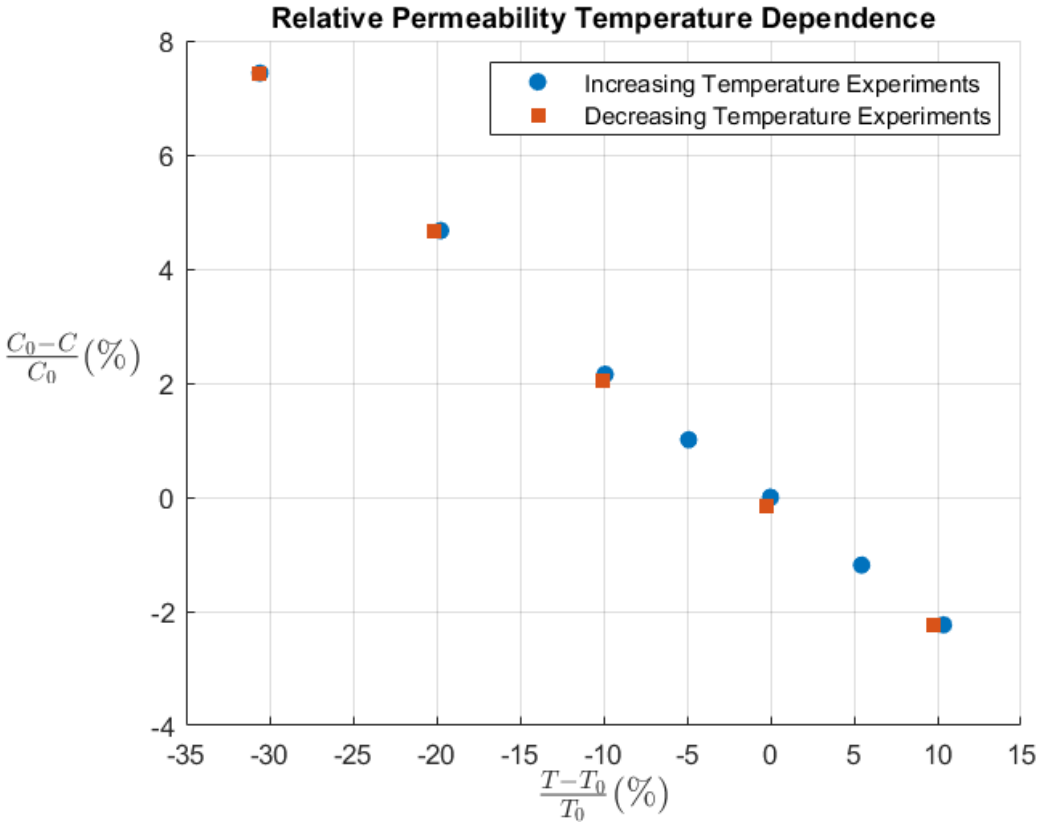

Figure 3.10 Temperature dependence of the filter permeability.

Experiments conducted on the degraded oil (Shell Rotella T6 5W-40) showed similar temperature dependence for the pressure drop across the filter complex (Figure 3.11). While there are subtle differences in the line of best fit for the clean oils and degraded oils, these studies cannot distinguish between the same. However, such studies are useful to calibrate the test facility and instrumentation whenever the working fluid is changed and to set up the facility for oil quality evaluation.

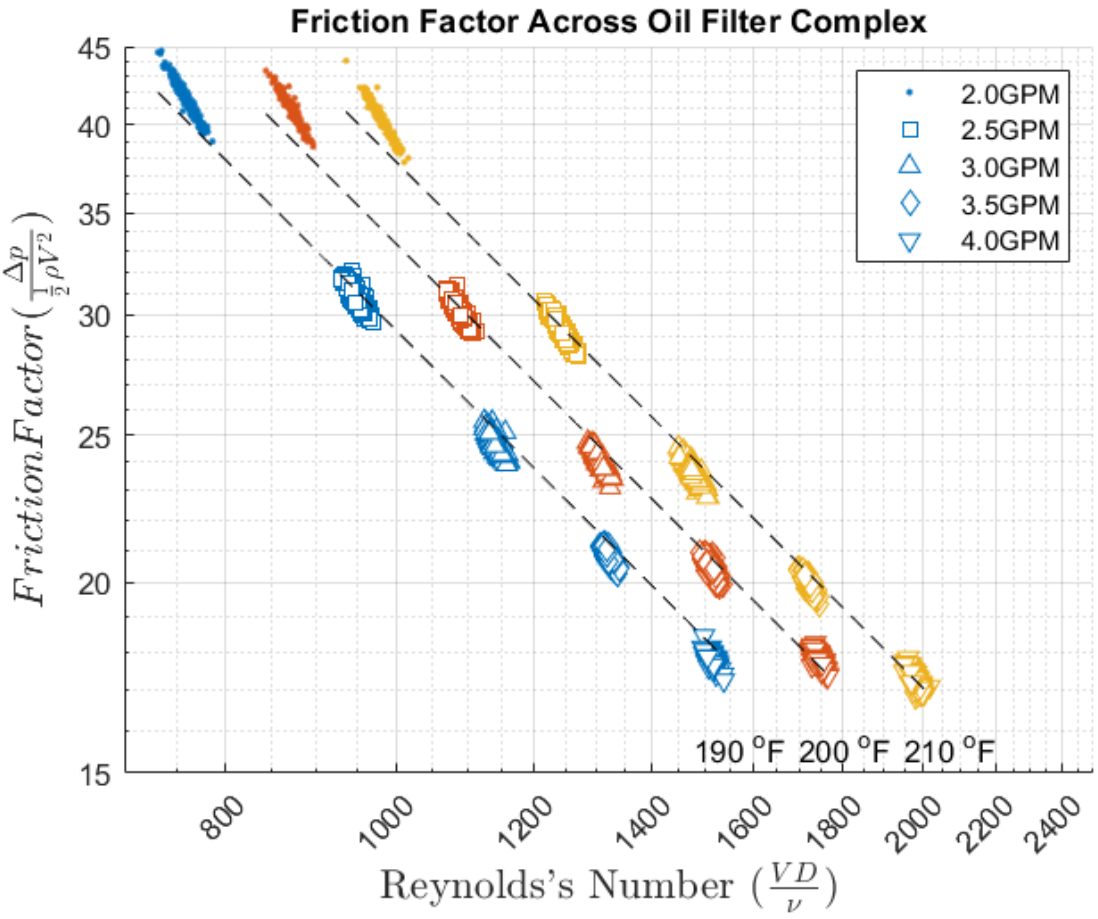

Figure 3.11 Filter housing complex friction factor data and developed equation for the degraded Shell Rotella T6 5W-40.

The state of the filters following the mentioned experiments are shown in Figure 3.12. While the filters used with clean oils show no visible changes, the one used with the degraded oil shows staining due to the capture of very fine suspended particles, whose presence does not impact the permeability characteristics of the filter.

(a) Virgin Ravenol HPS 5W-30.

(b) New Shell Rotella T6 5W-40.

(c) Degraded Shell Rotella T6 5W-40.

Figure 3.12 Appearance of oil filters used with different oils.

3.3 Oil Quality Studies

The OQS in the engine filter housing is angled 15° from the vertical, as it is the only possible configuration. The first study in the benchtop facility is to examine the role of orientation and its effects on the loss factor response. In these studies, the filter-mounted OQS response was compared to the response of a downstream OQS whose orientation was changed. These experiments were performed with degraded oil at 200 °F and 3.0 gpm flow rate. The downstream OQS was oriented to different positions from 0° to 180° in 45° increments (Figure 3.13). For these comparisons, the same OQS was used in both locations to eliminate any bias associated with different sensor calibrations. From here onward, the $tan(\delta)$ response from the OQS is referred to as the loss factor, commonly used by the industry that produces these sensors.

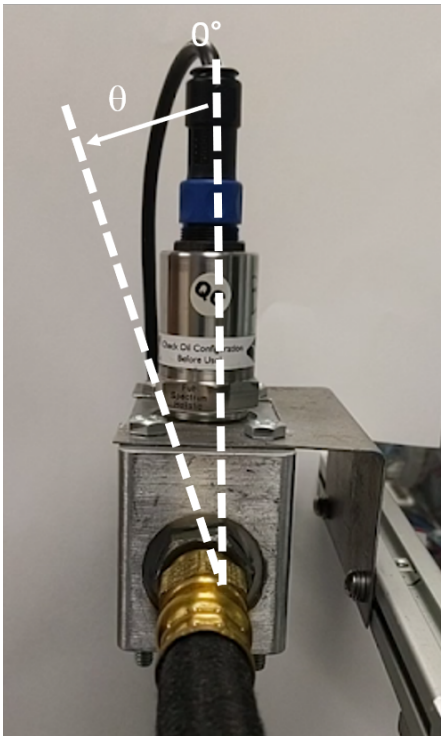

Figure 3.13 Schematic of the inline OQS that can be rotated about the axis of the hydraulic hose.

The data from the orientation studies of the degraded Shell Rotella T6 5W-40 oil measured at different angles by the inline OQS, and from the fixed postion filter-mounted OQS, are shown in Figure 3.14. From run to run, for given operating conditions, the OQS loss factor response demonstrated about ±0.25% loss factor uncertainty at a given orientation, whereas the variation for all orientations stayed within a ±0.5% uncertainty. It is also clear that the filter-mounted OQS in its 15° orientation and flow configuration measures oil quality with a high degree of precision. From a sensing perspective, it is still recommended that the OQS be oriented as close to vertical as possible, especially when sensing heavily degraded oils, as sedimentation and flow quality around the sensing elements could become problematic.

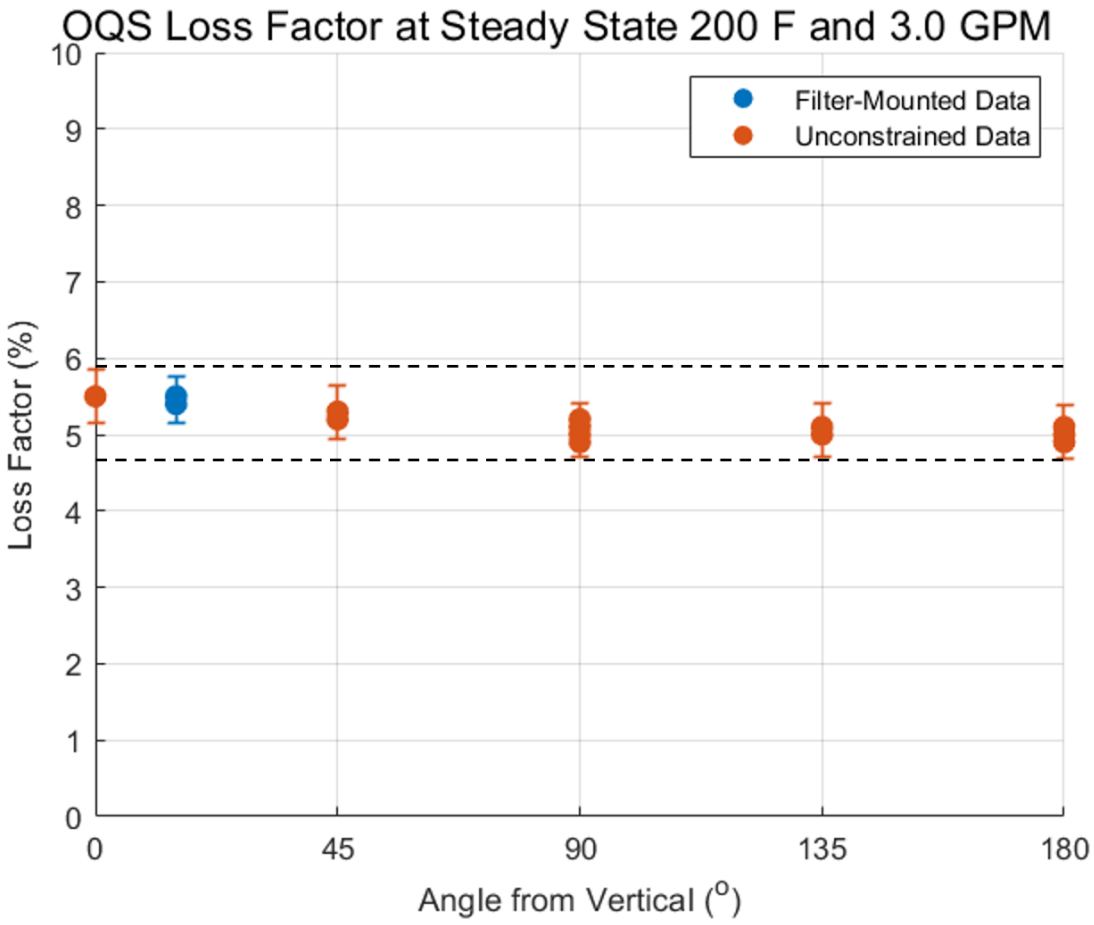

Figure 3.14 Inline OQS loss factor measurements at various angles compared to the fixed filter-mounted OQS for degraded Shell Rotella T6 5W-40.

Figure 3.15 shows another polar approach to data visualization for orientation studies that would be recommended for heavily degraded oils to establish any sedimentation and flow quality effects on sensing.

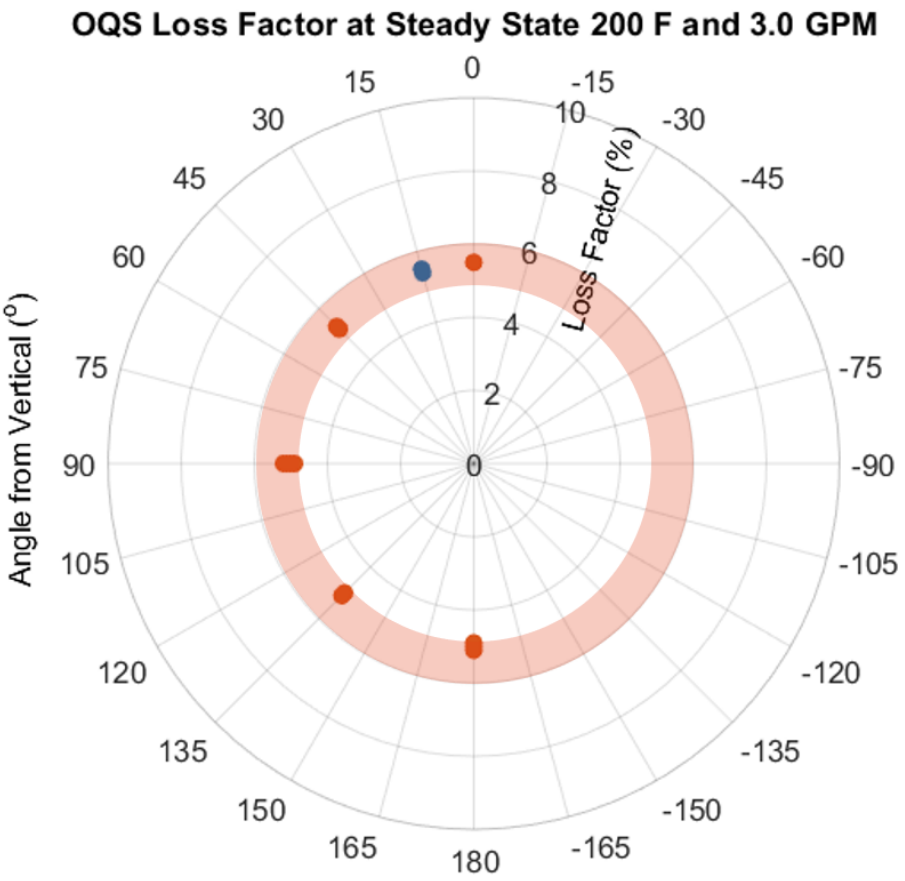

Figure 3.15 Alternate polar visualization of inline OQS loss factor measurements at various angles compared to the fixed filter-mounted OQS for degraded Shell Rotella T6 5W-40.

3.3.1 Oil Quality Measurement

Figure 3.16a shows that the oil quality loss factor measurement has no observable drift as the temperature is held steady over a period of 30 minutes. The oil quality sensor senses oil quality to a precision of ±0.1% loss factor. This time study is the first indication that such a sensor can be incorporated *in situ* for engine oil health monitoring.

Figure 3.16b shows run-run variation in oil quality loss factor measurement when the benchtop facility is switched on each time from ambient conditions to a set temperature. This shows that the loss factor measurement from the same OQS can vary by ±0.25% for different runs at the same operating conditions.

In these studies, temperature of the flow was interpreted using the Pt100 temper-

ature sensor downstream of the filter complex, as the temperature sensor embedded in the OQS had lower precision.

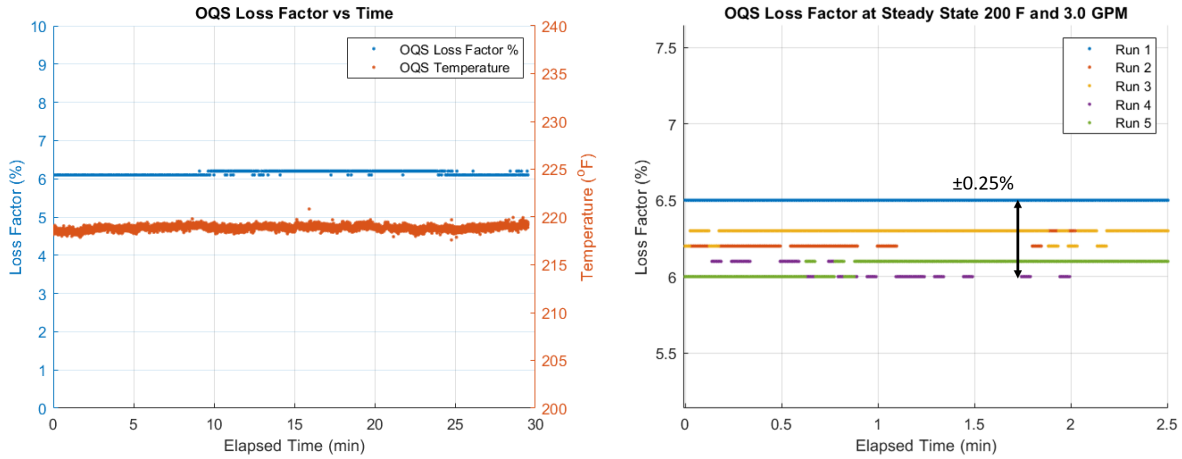

(a) OQS loss factor measurement at steady state.

(b) OQS loss factor measurement uncertainty.

Figure 3.16 OQS loss factor measurement behavior for the degraded Shell Rotella T6 5W-40.

Oil quality measurements are an indication of the state of oxidative degradation of the oil. As indicated in Section 1.4, the concentration of polar molecules increases with degradation and provides a mechanism to examine oil quality through measurement of $tan(\delta)$ values, which are a representation of permittivity of the oil. Since $tan(\delta)$ sensing is a measure of permittivity and permittivity increases with temperature, it is expected that the loss factor measurement will slightly increase with temperature. Figure 3.17 shows the loss factor increase as the temperature is incrementally increased from about 140 °F to 220 °F. In the experiment shown below, temperature was held steady for 10 minutes at each setpoint, allowing for sufficient time for the OQS loss factor measurement to reach steady state values.

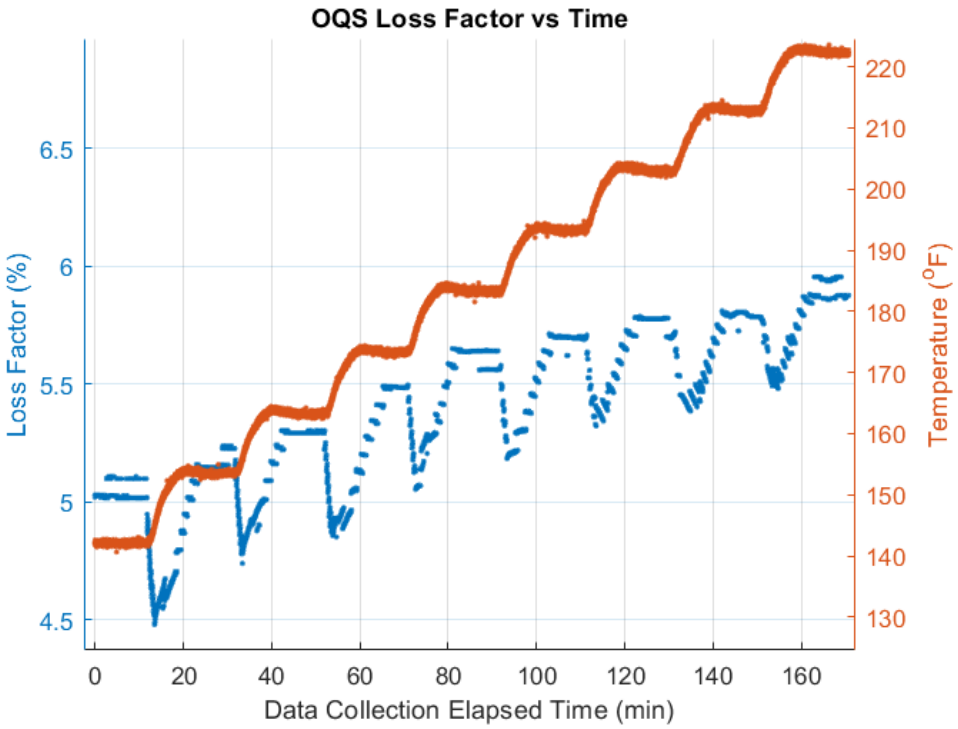

Figure 3.17 OQS measured loss factor response for both steady state and transient temperatures for the degraded Shell Rotella T6 5W-40.

Figure 3.18 shows the transient response of the OQS loss factor measurements to the toggling of temperature for both clean and degraded oils. It is observed that the OQS has a long time constant before it reaches a steady state value. During the period of temperature change, the OQS's loss factor response does not accurately map with the temperature, likely an artifact stemming from the design and performance of the embedded electronics and software.

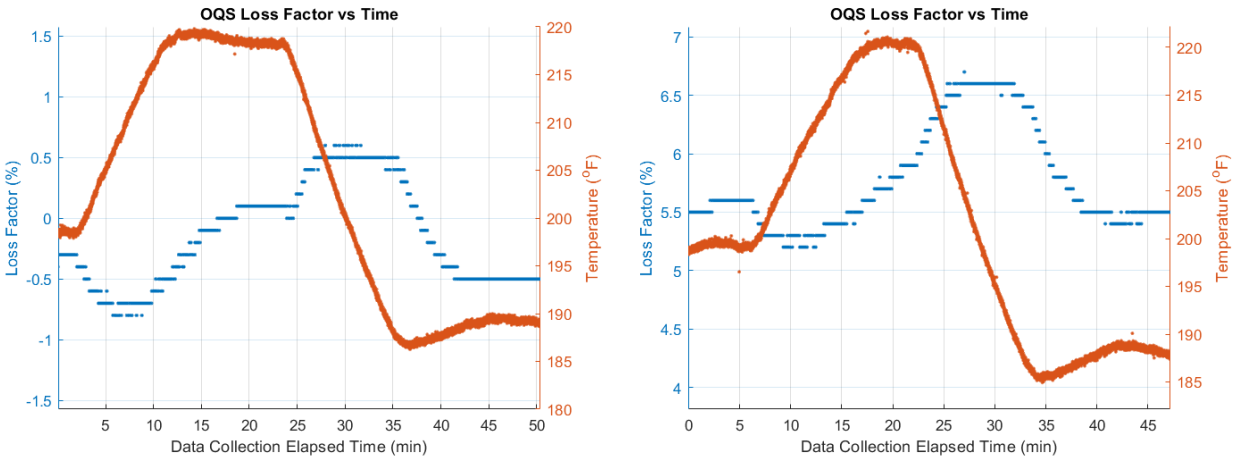

(a) Virgin Ravenol HPS 5W-30. **(b)** Degraded Shell Rotella T6 5W-40.

Figure 3.18 OQS loss factor response at transient temperatures.

Figure 3.19 captures the response of the OQS as the facility temperature is ramped up from room temperature to operating conditions of 200 °F, again emphasizing that if the OQS were incorporated for *in situ* engine measurements, there is a substantial waiting period before OQS loss factor measurements can be interpreted for engine oil health monitoring.

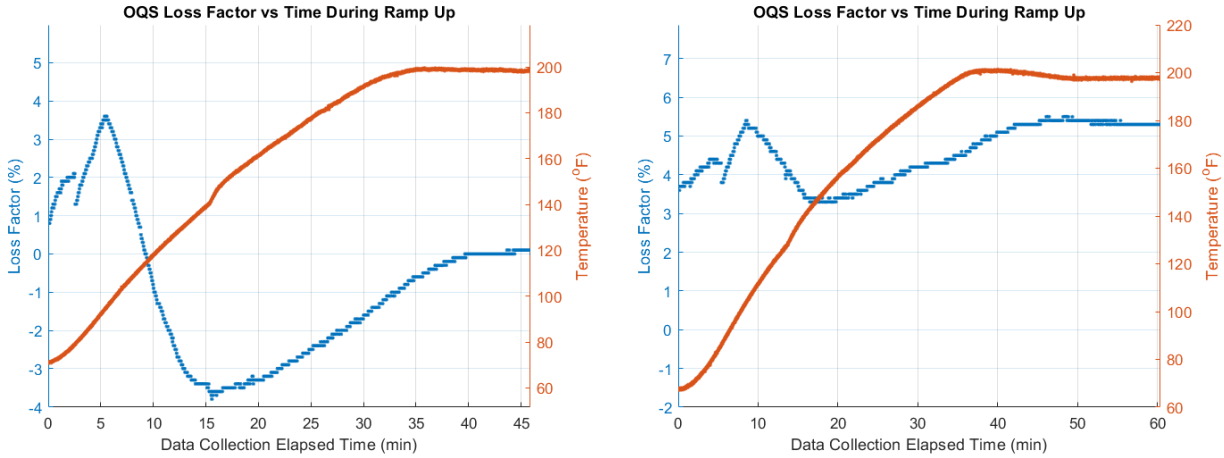

(a) Virgin Ravenol HPS 5W-30. **(b)** Degraded Shell Rotella T6 5W-40.

Figure 3.19 OQS loss factor response during ramp up from room temperature to operating temperature.

3.3.2 Projecting Oil Quality at Operating Conditions

A detailed study to examine temperature dependence of the loss factor response was done in which 10 minutes of steady state data were recorded at temperatures from 90 °F to 230 °F in 5 °F increments, accomplished over several runs on different days (Figure 3.20).

The scope of these studies was to examine whether room temperature loss factor measurements can be used to project loss factor measurements at engine operating temperatures. This is necessitated by the fact that it could be expensive to incorporate an OQS on every engine in a fleet, whereas it is relatively easy to dip an OQS into a sample of engine oil and take a measurement at room temperature.

From Figure 3.20, it is clear that beyond 140 °F, the loss factor response of the OQS mirrors the expected permittivity increase with temperature. However, below 140 °F, the steady-state loss factor response of the OQS does not follow any physical correlations. If it is desired to make predictions using room temperature measurements, then machine learning approaches have to be used, as the observations are beyond the scope of traditional physics.

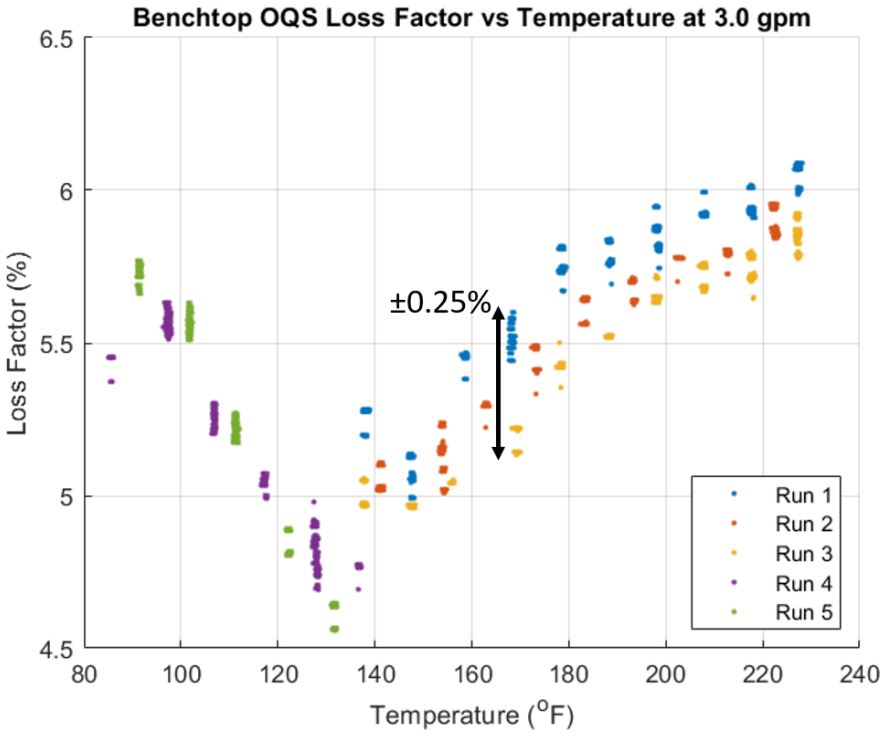

Figure 3.20 OQS loss factor temperature response and repeatability for equivalent steady state conditons of the degraded Shell Rotella T6 5W-40.

Replotting data from previous studies shows that $tan(\delta)$ has a logarithmic temperature dependence [21]. This is to be expected because conductivity increases with temperature; however, this increase is a slow increase best captured by a logarithmic dependence. A logarithmic model of the form shown in Equation 3.7, with a reference temperature T_0 in °F and constants A and B, best fits the loss factor response in the range of engine operating temperatures. For these data, a temperature of 140 °F was chosen as the reference.

$$lossfactor = Aln(\frac{T}{T_0}) + B \tag{3.7}$$

Best fit equations of this form were found for steady state data collected between 140 °F and 235 °F (Figure 3.21). This demonstrates that the loss factor of a given engine oil at operating temperature (about 180 °F to 240 °F) can be predicted if measurements are made at a temperature such as 140 °F instead of room temperature. Such a temperature can be easily achieved in an laboratory setting by placing an oil sample in a temperature-controlled bath. It is expected that similar temperature dependence will be found for oils of various levels of degradation, though the constants A and B will be different.

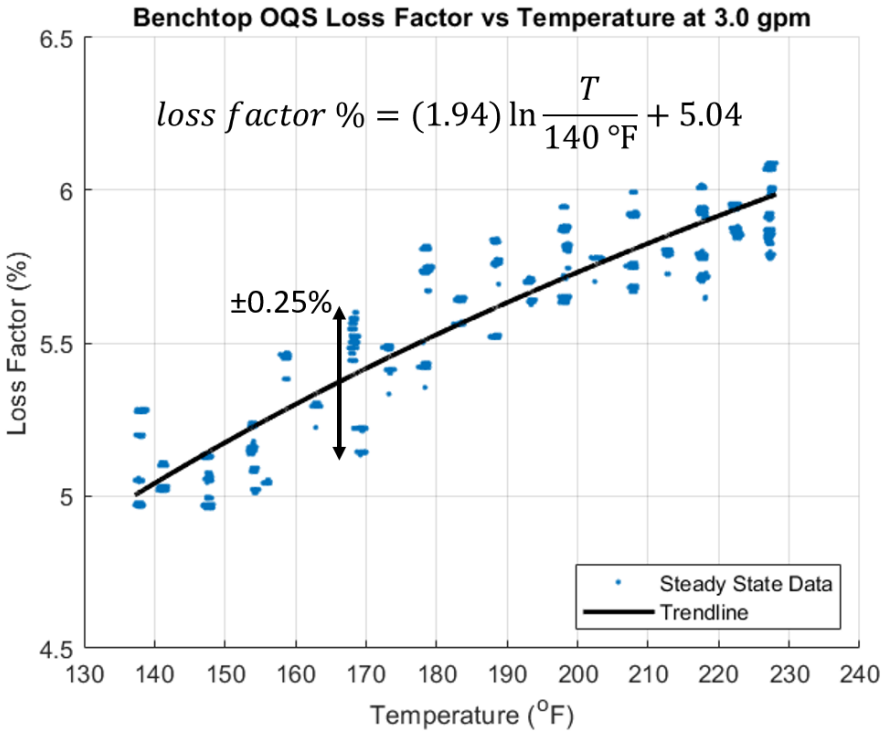

Figure 3.21 Model for loss factor temperature dependence for the degraded Shell Rotella T6 5W-40.

It may be possible to use the power of projection through machine learning methods to predict the loss factor response at engine operating conditions through measurements at room temperatures. UThe continuous line in Figure 3.22 shows a projection model developed using Support Vector Regression (SVR) using the current data to predict operating temperature loss factor given a room temperature measurement. This analysis was provided by Yubo Du, a graduate student at Vanderbilt University affiliated with the project. Such a model can be potentially used by field operators to diagnose engine oil condition from a sample.

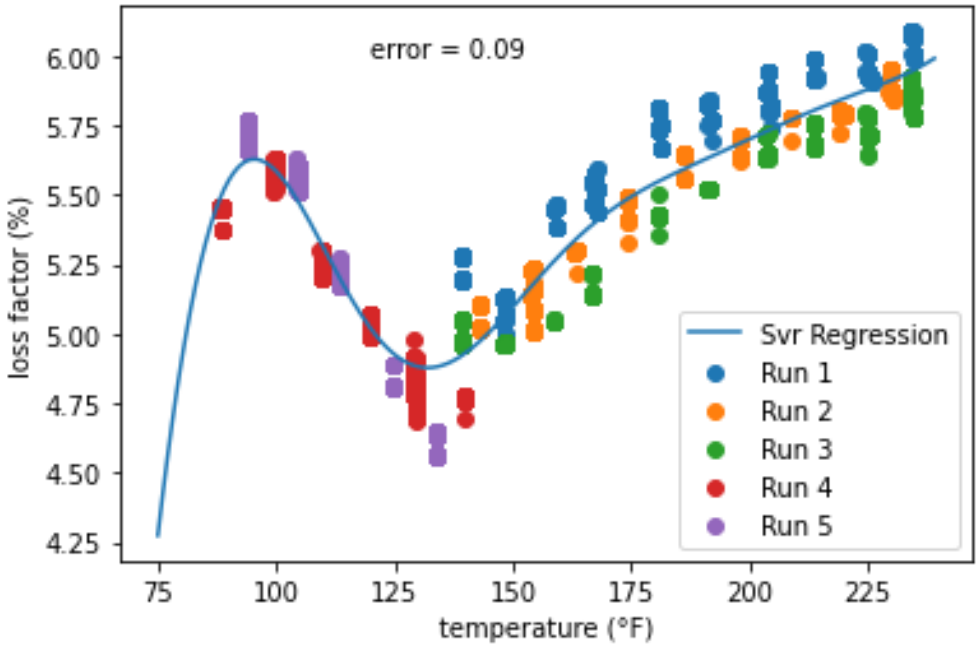

Figure 3.22 Machine learning model for loss factor temperature dependence for the degraded Shell Rotella T6 5W-40 (courtesy of Yubo Du).

CHAPTER FOUR

CONCLUSION

In situ oil quality sensing could become a standard in the transportation industry as it moves toward optimal utilization of natural resources. This technique provides a use-based assessment of oil quality which could replace traditional mileage and hour-based approaches to recommend engine oil changes. Its immediate application is in the marine industry where no such land-based analogues can be used to assess an engine oil's quality and need for replacement. For an end user with a large fleet, *in situ* oil quality monitoring could thereby lead to substantial savings in maintenance costs and labor.

In this study, a precision benchtop facility for circulating engine oil was designed, built, and tested for parametric evaluation of an oil quality sensor's measurement capabilities. This facility has the ability to independently control temperature, flow rate, and OQS orientation and has precision pressure and temperature sensors to interrogate the flow. It duplicates engine operating conditions and has an oil filter in the line and can examine engine oils of varying viscosity grades and levels of degradation.

Oil quality sensing is dependent on the measured change in an engine oil's permittivity with usage. Oxidative degradation of an engine oil at the harsh high-temperature and high-pressure environment of the piston-cylinder interface produces polar molecules that alter the oil's permittivity. The state-of-the-art oil quality sensors sense in the MHz frequency range to provide a robust and reliable response.

The current research systematically evaluated an oil quality sensor in the benchtop facility, for two oils of different levels of degradation, by varying the operating temperature and flow rate and by changing the oil quality sensor spatial orientation. The results establish that the new generation of oil quality sensors are orientation-agnostic, offer precise and repeatable measurements of oil quality, and are therefore reliable for deployment.

Two scientific tasks were undertaken for this assessment: the use of fluid dynamics techniques to categorize the oil flow in the loop and the development of projection models to predict engine oil quality loss factor values at engine operating temperatures from room

temperature measurements.

Results from the first task showed that the fluid flow through the oil filter complex was viscous and well-captured by dimensional analysis techniques and resulting representations. During the process of analyzing the data, it was discovered that the permeability of the filter changes with temperature. In a constrained volume, any expansion of the filter material leads to a decrease in porosity and increases the filter permeability and flow resistance across the filter. Such studies are an essential first step to calibrate the facility and setting it up for oil quality evaluation.

Results from the second task established that loss factor measurements of an engine oil sample at a manageable 140 °F can be used to project loss factor measurements at engine operating temperatures of 180 °F to 240 °F. These measurements vary with the state of degradation of an engine oil and are a weak function of temperature; this is well-captured by the experimental results, which show loss factor as a logarithmic function of temperature.

However, loss factor measurements by the OQS are inconsistent below 140 °F as a consequence of proprietary embedded hardware and software factors beyond the scope of this investigation. In this context, a purely physics-based model is unable to project loss factor measurements below 140 °F.. If it intended for end users to be able to project loss factor values from room temperature measurements, machine learning approaches could provide a useful tool. This, along with the measurement of other functional parameters such as engine vibration characteristics, provides a platform for a truly autonomous and intelligent engine health monitoring system.

Through the parametric evaluation of the performance of an *in situ* oil quality sensor, the fundamental studies of this investigation have laid the foundation for further developments in engine health monitoring, whether the end-use application is automotive, marine, or industrial diesel engines.

REFERENCES

[1] Eckard Irion, Klaus Land, Thomas Gürtler, and Manfred Klein. "Oil-Quality Prediction and Oil-Level Detection with the TEMIC QLT-Sensor Leads to Variable Maintenance Intervals". In: *SAE Transactions. Journal of Passenger Cars* 106 (1997), pp. 1390–1395. URL: https://www.jstor.org/stable/44731294.

[2] TongHai Wu, HongKun Wu, Ying Du, and ZhongXiao Peng. "Progress and trend of sensor technology for on-line oil monitoring". In: *Science China Technological Sciences* 56.12 (Oct. 2013), pp. 2914–2926. DOI: 10.1007/s11431-013-5400-5. URL: https://doi.org/10.1007/s11431-013-5400-5.

[3] Matthew Appleby, Fred K. Choy, Li Du, and Jiang Zhe. "Oil debris and viscosity monitoring using ultrasonic and capacitance/inductance measurements". In: *Lubrication Science* 25.8 (Feb. 2013). DOI: 10.1002/ls.1221. URL: https://doi.org/10.1002/ls.1221.

[4] Zhibin Han, Yishou Wang, and Xinlin Qing. "Characteristics Study of In-Situ Capacitive Sensor for Monitoring Lubrication Oil Debris". In: *Sensors(Basel, Switzerland)* 17.12 (Dec. 2017), p. 2851. DOI: 10.3390/s17122851. URL: https://doi.org/10.3390/s17122851.

[5] Amiyo Basu, Axel Berndorfer, Carlos Buelna, James Campbell, Keith Ismail, Yingjie Lin, Lorenzo Rodriguez, and Simon S. Wang. ""Smart sensing" of Oil Degradation and Oil Level Measurements in Gasoline Engines". In: *SAE Transactions. Journal of Fuels and Lubricants* 109 (2000), pp. 857–863. URL: https://www.jstor.org/stable/44745894.

[6] Heiko Dobrinski, Andreas Buhrdorf, Olaf Lüdtke, and Uwe Knipper. "Multiparameter Oil Condition Sensor Based on the Tuning Fork Principle". In: *SAE Transactions. Journal of Passenger Cars: Electronic and Electrical Systems* 116 (2007), pp. 13–22. URL: https://www.jstor.org/stable/44719863.

[7] Milton D. Johnson, Stefan Korcek, and Kurt Schriewer. "In-Service Engine Oil Condition Monitoring - Opportunities and Challenges". In: *SAE Transactions. Journal of Fuels and Lubricants* 103 (1994), pp. 1727–1734. URL: https://www.jstor.org/stable/44612457.

[8] John Manyala and Massood Atashbar. "On-Line Lubricants Health Condition Monitoring in Gearbox Application". In: *SAE International Journal of Fuels and Lubricants* 6.3 (2013), pp. 907–914. DOI: 10.4271/2013-01-9074. URL: https://doi.org/10.4271/2013-01-9074.

[9] J. Siegel, R. Bhattacharyya, A. Deshpande, and S. Sarma. "Vehicular engine oil service life characterization using On-Board Diagnostic (OBD) sensor data". In: SENSORS, 2014 IEEE. Valencia, Spain: IEEE, 2014, pp. 1722–1725. DOI: 10.1109/ICSENS.2014.6985355. URL: https://doi.org/10.1109/ICSENS.2014.6985355.

[10] Shady Mohamed, Vu Le, Chee Peng Lim, Saeid Nahavandi, Leong Yen, Guy Edward Gallasch, Stephen Baker, David Ludovici, Nick Draper, and Vish Wickramanayake. "Condition monitoring of engine lubrication oil of military vehicles: a machine learning approach". In: AIAC 2017 : Proceedings of the 17th Australian International Aerospace Congress. Melbourne, Victoria, Australia: Australian Defence Science and Technology Group, 2017, pp. 1–7.

[11] Phil Ramsey. *Around and Around - Where the Oil Goes in Your Engine*. Machinery Lubrication. Sept. 2003. URL: https://www.machinerylubrication.com/Read/532/around-around-where-oil-goes-in-your-engine.

[12] Artur Wolak. "Sieving hydrogen isotopes through two-dimensional crystals". In: *Measurement and Control* 51.3–4 (Apr. 2018), pp. 65–72. DOI: 10.1177/0020294018770916. URL: https://doi.org/10.1177/0020294018770916.

[13] Sam George, Santhosh Balla, Vishaal Gautam, and Mridul Gautam. "Effect of diesel soot on lubricant oil viscosity". In: *Tribology International* 40.5 (May 2007), pp. 809–818. DOI: 10.1016/j.triboint.2006.08.002. URL: https://doi.org/10.1016/j.triboint.2006.08.002.

[14] Marie Sejkorová, Ivana Hurtová, Josef Glos, and Jan Pokorný. "Definition of a Motor Oil Change Interval for High-Volume Diesel Engines Based on its Current Characteristics Assessment". In: *Acta Univ. Agric. Silvic. Mendelianae Brun.* 65.2 (Apr. 2017), pp. 481–490. DOI: 10.11118/actaun201765020481. URL: https://doi.org/10.11118/actaun201765020481.

[15] Gus Wright. *Fundamentals of Medium/Heavy Duty Diesel Engines*. Jones & Bartlett Learning, Dec. 2015. Chap. 12, p. 345. ISBN: 9781284067057.

[16] ASTM Standard D341-20e1. *Standard Practice for Viscosity-Temperature Equations and Charts for Liquid Petroleum or Hydrocarbon Products*. Standard. West Conshohocken, PA: ASTM International, 2020. DOI: 10.1520/D0341-20E01. URL: https://doi.org/10.1520/D0341-20E01.

[17] F. Xavier Borras, Matthijn B. De Rooij, and Dik J. Schipper. "Rheological and Wetting Properties of Environmentally Acceptable Lubricants (EALs) for Application in Stern Tube Seals". In: *Lubricants* 6.4 (2018), p. 100. DOI: 10.3390/lubricants6040100. URL: https://doi.org/10.3390/lubricants6040100.

[18] James S. Dickmann, Mark T. Devlin, John C. Hassler, and Erdogan Kiran. "High Pressure Volumetric Properties and Viscosity of Base Oils Used in Automotive Lubricants and Their Modeling". In: *Industrial & Engineering Chemistry Research* 57.50 (Nov.

2018), pp. 17266–17275. DOI: 10.1021/acs.iecr.8b03484. URL: https://doi.org/10.1021/acs.iecr.8b03484.

[19] Anand Kumar Tripathi and Ravikrishnan Vinu. "Characterization of Thermal Stability of Synthetic and Semi-Synthetic Engine Oils". In: *Lubricants* 3.1 (2015), pp. 54–79. DOI: 10.3390/lubricants3010054. URL: https://doi.org/10.3390/lubricants3010054.

[20] Constantine T. Dervos, Christos D. Paraskevas, Panayotis D. Skafidas, and Panayota Vassiliou. "A Complex Permittivity Based Sensor for the Electrical Characterization of High-Voltage Transformer Oils". In: *Sensors* 5.4 (2005), pp. 302–316. DOI: 10.3390/s5040302. URL: https://doi.org/10.3390/s5040302.

[21] M. Pecovska-Gjorgjevich, A. Andonovski, and J. Velevska. "Measuring Frequency and Temperature-Dependent Permittivities of Vegetable Oils". In: *Physica Macedonica* 59 (2011), pp. 77–89. URL: https://www.researchgate.net/publication/233816928_Measuring_frequency-_and_temperature-dependent_permittivities_of_vegetable_oils.

[22] Angel Torres Pérez and Mark Hadfield. "Low-Cost Oil Quality Sensor Based on Changes in Complex Permittivity". In: *Sensors* 11.11 (2011), pp. 10675–10690. DOI: 10.3390/s111110675. URL: https://doi.org/10.3390/s111110675.

[23] Christopher John Collister. "Electrical Measurement of Oil Quality". US6459995B1. 1998.

[24] *Oil Condition Sensor OCS and Accessories. Stauff*. Global Resources, Inc. URL: https://www.gsglobalresources.com/uploads/Oil_Condition_Sensor_OCS-Accessories_Manual_EN-web.pdf.

[25] Ahmad K. Sleiti. "Heat transfer measurements of Polyalpha-Olefin- boron nitride nanofluids for thermal management and lubrication applications". In: *Case Studies in Thermal Engineering* 22 (Dec. 2020), p. 100776. DOI: 10.1016/j.csite.2020.100776. URL: https://doi.org/10.1016/j.csite.2020.100776.

[26] Lalit Kumar Bohra, Leo M. Mincks, and Srinivas Garimella. "Experimental Investigation of Pressure Drop Characteristics of Viscous Fluid Flow Through Small Diameter Orifices". In: *ASME Journal of Fluids Engineering* 143 (2 Feb. 2021), p. 021306. DOI: 10.1115/1.4048617. URL: https://doi.org/10.1115/1.4048617.

[27] Hujo L'ubomír, Jablonický Juraj, Markovič Jaromír, Tulík Juraj, Simikić Mirko, Zastempowski Marcin, and Janoušková Romana. "Design of Laboratory Test Equipment for Automotive Oil Filters to Evaluate the Technical Life of Engine Oil". In: *Applied Sciences* 11 (2 Jan. 2021), p. 483. DOI: 10.3390/app11020483. URL: https://doi.org/10.3390/app11020483.

APPENDIX A

DATA PROCESSING

A National Instruments USB-6212 was used to collect signals from everything but the OQS, which was supplied with a USB cable that was connected to the computer. This data acquisition board was referenced to the system common ground. All of the twisted wire pairs were made with BNC terminations. All measurements were configured as single-ended inputs referenced to ground except those measuring the voltage across the Pt100 temperature sensors, which were configured as a differential inputs. The board was minimally configured to collect continuous samples at a sampling rate of 500 Hz to satisfy the Nyquist criterion for the expected frequencies and was updated to read 1200 samples per iteration at sampling rate of 5 kHz.

Figure A.1 shows the block diagram of the LabVIEW software used to interface with the data acquisition board. Factory calibration values are used to calculate the measurement of each sensor. The RMS value with a buffer size of 100 was used for recording pressure measurements. All measurements were written to a text file. A user-friendly front panel, shown in Figure A.2, simplified data collection and observation of facility status.

All LabVIEW and OQS data recorded to text files were used in a 2,000 line MATLAB post-processing script that parametrized all variables to simplify analysis and plotting for any experiment or oil type.

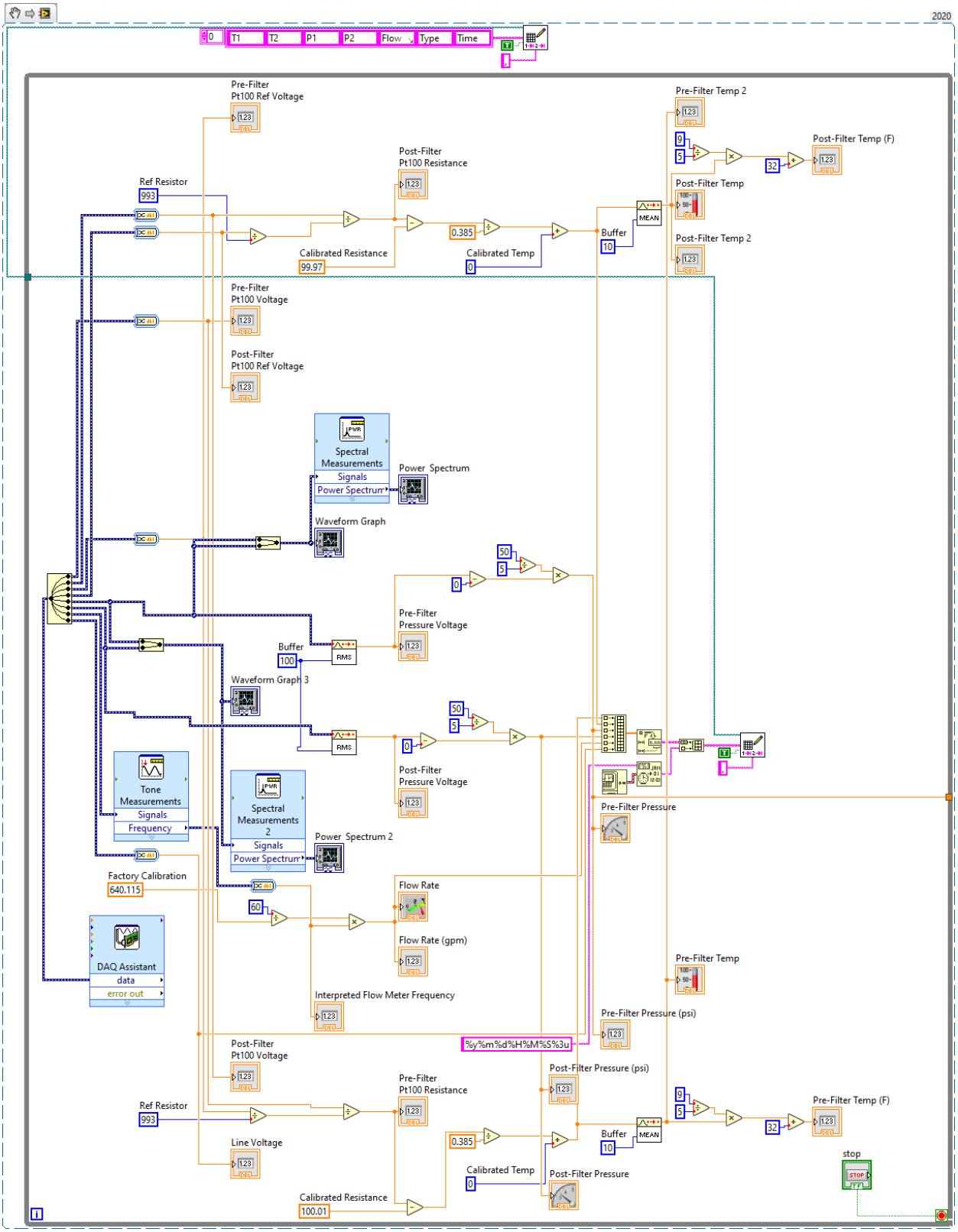

Figure A.1 LabVIEW block diagram for data collection.

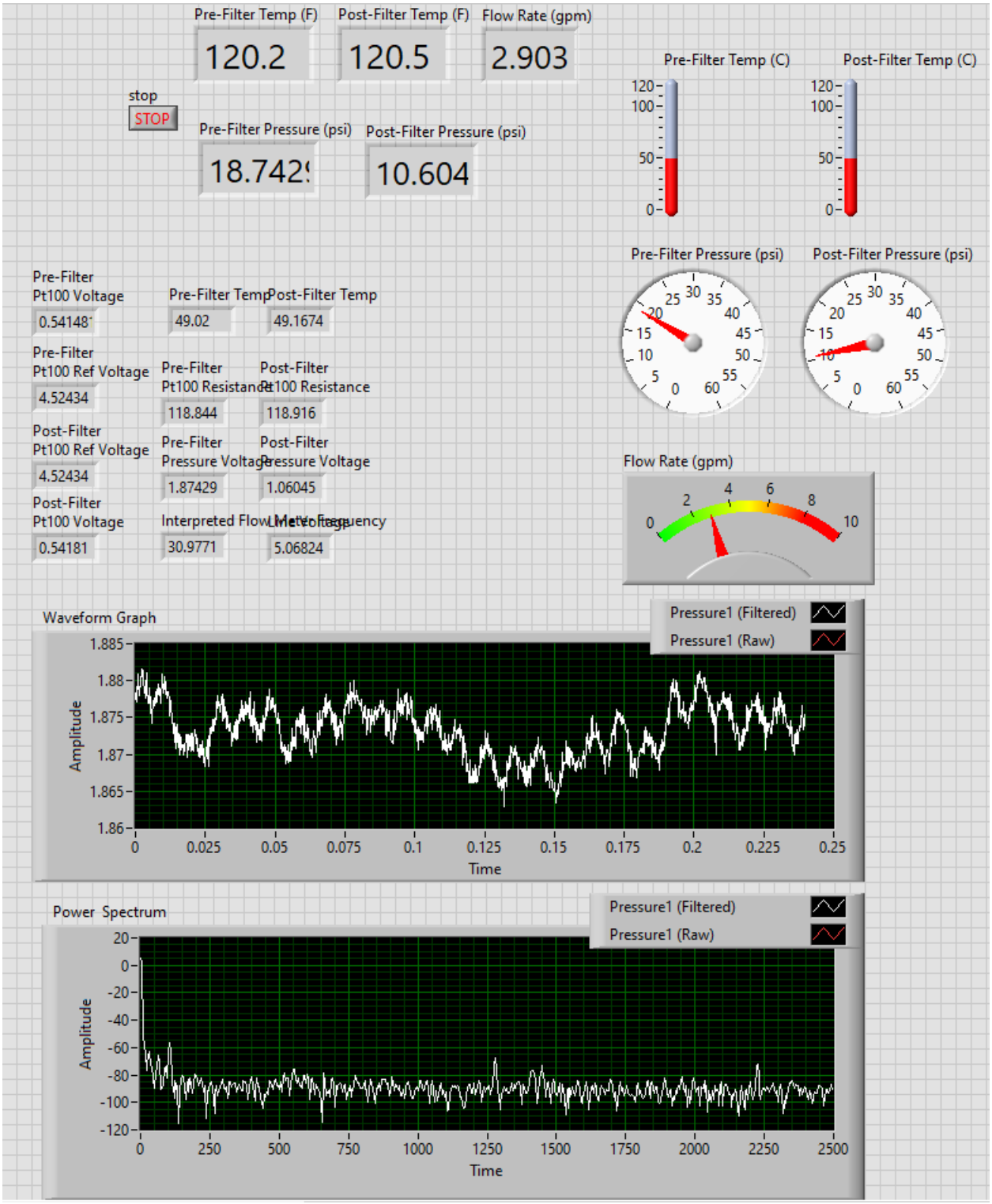

Figure A.2 LabVIEW front panel for data collection.

APPENDIX B

FLOW METER CALIBRATION

FLOMEC™ A1908023

FLOWMETER CALIBRATION CERTIFICATE

FLOWMETER PRIMARY DATA

Flowmeter Type:	Positive Displacement	Calibration Date:	07-March-2019
Model Number:	OM015A001-822G	Cert. Revision No:	-
Serial Number:	A1908023	Tag Number:	

SECONDARY INSTRUMENT DATA

Model Number:	
Serial Number:	

CALIBRATION RESULTS

Flow Rate		Volume	Pulses Recorded	
Litres / min	*US Gal/min*	*Litres*	Output 1	Output 2
15.00	3.96	30.130	5095	2548

METER K-FACTORS

Output	Type	K-Factor (Pulses/L)	K-Factor (Pulses/G)
1	Hall Effect Sensor	**169.101**	**640.115**
2	Reed Switch	**84.567**	**320.120**
3	N/A		

VOLUME STANDARD

Method:	Master Meter *	Model Number:	Flomec OM025S	
Test Media:	Mineral oil**	ID Number:	MM004-3	
Oil Viscosity:	3 - 5 cP	Oil Temperature:	20 ºC	68 ºF

* Master meter has been calibrated to internal procedures against NATA traceable equipment, in accordance with AS4250.5-1995

** Castrol Diesel Calibration Fluid 4113 is used for all calibrations - product datasheet and MSDS are available on request

GREAT PLAINS INDUSTRIES AUSTRALIA GPI

Trimec Industries Pty Ltd, ABN 93 003 381 477, operating as Great Plains Industries Australia

1/16 Atkinson Road (PO Box 2444), Taren Point, NSW, 2229, Australia

T +61 (0)2 9540 4433 / F +61 (0)2 9525 9411 / flomec.com.au

Certified System Quality ISO 9001

Figure B.1 Flomec flow meter calibration sheet.

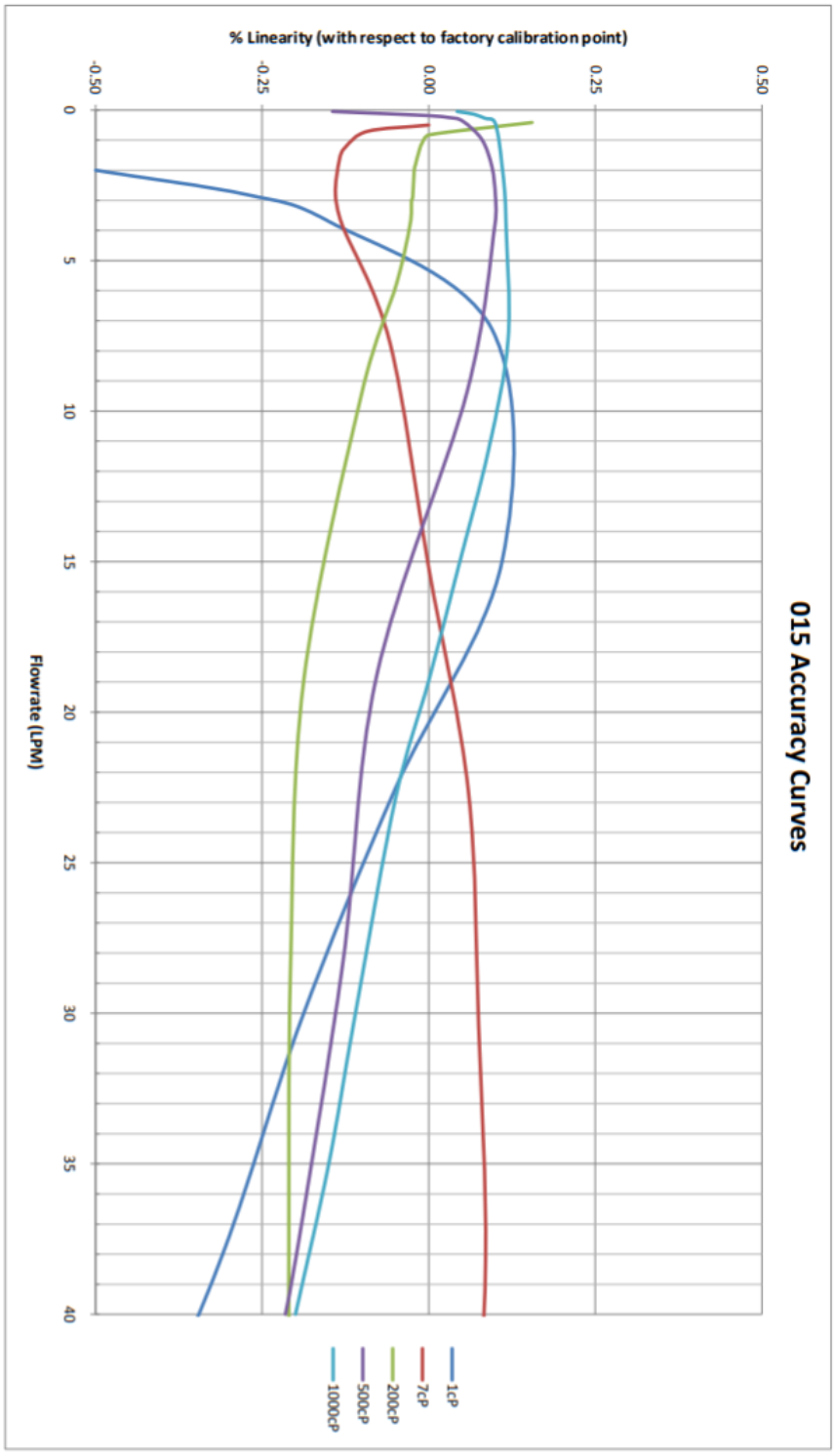

Figure B.2 Flomec flow meter accuracy curves.

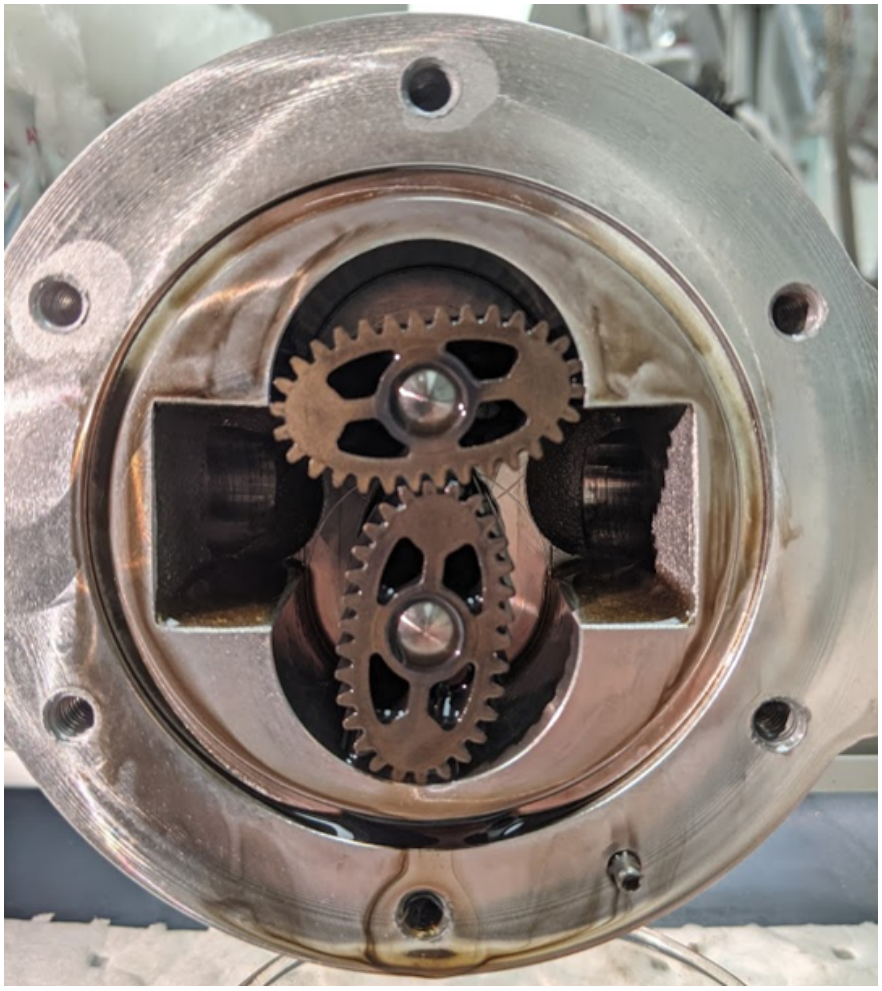

Figure B.3 Internal inspection of Flomec flow meter.